JOURNAL OF GEOPHYSICAL RESEARCH, VOL. 103, NO. C7, PAGES 14,241–14,259, JUNE 29, 1998

On the structure and evolution of ENSO-related climate variability in the tropical Pacific: Lessons from TOGA

J. M. Wallace,[1] E. M. Rasmusson,[2] T. P. Mitchell,[1] V. E. Kousky,[3] E. S. Sarachik,[1] and H. von Storch[4]

Abstract. Improved observations in the tropical Pacific during the Tropical Ocean-Global Atmosphere (TOGA) program have served to corroborate preexisting notions concerning the seasonally dependent relationships between sea surface temperature, sea level pressure, wind stress, rainfall, upper tropospheric circulation, and ocean thermal structure anomalies in the El Niño-Southern Oscillation (ENSO) phenomenon. However, the paradigm of a quasiperiodic "ENSO cycle," phase locked with the annual march, does not capture the complexity of the evolution of the anomalies. The inadequacy of this model was particularly apparent during the second half of TOGA when the variability was highly aperiodic. Also, a single modal structure or empirical orthogonal function does not appear to be capable of representing the range of spatial patterns of ocean-atmosphere interaction in the tropical Pacific. These results suggest the need for a more inclusive phenomenological description of ENSO. Data collected during TOGA serve to confirm the influence of tropical Atlantic sea surface temperature anomalies upon rainfall in northeast Brazil.

1. Introduction

A distinguishing characteristic of the Tropical Ocean-Global Atmosphere (TOGA) program was its strong phenomenological focus. It was inspired and molded by the scientific community's perceptions that (1) the El Niño-Southern Oscillation phenomenon (ENSO) is the primary source of global interannual climate variability, (2) ENSO owes its existence to coupled ocean-atmosphere interactions in the tropical Pacific, and (3) the coupled system exhibits a degree of predictability on the seasonal-to-interannual timescale. This article begins with a review of the observations, the scientific investigations, and the climate events that gave rise to these perceptions, with emphasis on phenomena in the tropical Pacific. This historical background is followed in section 3 by a documentation of the ENSO-related variability in the tropical Pacific during the TOGA decade. Section 4 surveys large-scale, coupled ocean-atmosphere interaction in the tropical Atlantic and Indian Oceans. The final section reflects upon how the observations taken during the TOGA decade have modified preexisting notions concerning the structure and evolution of the ENSO phenomenon, in particular, and coupled tropical ocean-global atmosphere variability, in general.

2. Historical Background

The recognition of ENSO as a coupled ocean-atmosphere phenomenon and the appreciation of its important role in seasonal-to-interannual climate variability were not the result of a single dramatic scientific "breakthrough"; rather, they developed out of a series of studies spanning a period of more than six decades.

2.1. Early Investigations

The first significant step toward the recognition and understanding of ENSO was a study by *Brooks and Braby* [1921], who noticed that long-lasting wet and dry regimes at island stations in the western and central equatorial Pacific tend to be spatially coherent across a broad longitude belt and associated with interannual variations in the surface wind field. It is now clear that this relationship between the equatorial Pacific easterlies and rainfall is a fundamental feature of ENSO variability.

Three years later, *Walker* [1924] published the landmark synthesis of his studies of coherent global variability, in which he described the broadscale characteristics of the Southern Oscillation in terms of the sea level pressure (SLP), surface temperature, and rainfall variability. The linkage between the equatorial Pacific variations discovered by *Brooks and Braby* [1921] and the Southern Oscillation (SO) was forged a decade later in a paper entitled "Marquesan Meteorology" by *Leighly* [1933], which was truly remarkable for its time. It included a discussion of the relationship between year-to-year rainfall variations in the Marquesas Islands (centered near 10°S, 140°W) and climate anomalies in the equatorial trough zone (i.e., the belt of low SLP separating the subtropical anticyclones of the northern and southern hemispheres). Leighly deduced the fundamental relationship between sea surface temperature (SST) gradient, surface wind, and rainfall from simple two-station SLP differences, long before Darwin, Australia (12°S, 131°E) and Tahiti (17°S, 150°W) data began to be used routinely to monitor the SO. The fact that Leighly did not have access to SST data makes his deductions all the more impressive. His insight is well illustrated by the following quotation [*Leighly*, 1933, p. 164]:

> If, as may reasonably be concluded, the temperature of the ocean surface varies inversely with the force of the east winds of the

[1] Joint Institute for the Study of the Atmosphere and Ocean, University of Washington, Seattle.
[2] Department of Meteorology, University of Maryland, College Park.
[3] NOAA/NCEP Climate Prediction Center, Washington, D. C.
[4] Institute of Hydrophysics, GKSS, Geesthacht, Germany.

Paper number 97JC02905.
0148-0227/98/97JC-02905$09.00

> equatorial belt, periods of steep (surface pressure) gradient westward should also be periods of low water temperature, and thus unfavorable to rain on the mid-Pacific islands. This consideration supplies an explanation of the association of low temperature and drought, and conversely of high temperature and abundant rain. In the absence of further observational data on oceanic temperature, relative importance cannot be assigned to atmospheric circulation and water surface temperature as factors in the determination of rainfall fluctuations in the Marquesas. Since the two factors operate in conjunction, and result from the same fundamental causes, their effects would be difficult to separate.

Unfortunately, the lack of citations of this remarkable paper indicates that it had little or no impact on the field at the time. It appears that the first citation of Leighly's paper did not occur until *Julian and Chervin* [1978] recognized its significance in the context of their review of the SO and Walker Circulation phenomenon.

Following upon several decades of relatively weak and irregular behavior, ENSO-related climate variability became stronger and more cyclic in the 1950s, attracting renewed interest. The major warming of 1957–1958 was studied by *Ichiye and Peterson* [1963], who were the first to hypothesize that ocean-atmosphere interaction determines the evolution of the wind, SST, and rainfall fields in the equatorial Pacific. *Berlage* [1966] recognized the linkage between the SO and the episodic warmings of SST along the coast of southern Ecuador and northern Peru, known locally as El Niño [*Eguiguren,* 1894; *Murphy*, 1926; *Lobell*, 1942]. Another notable contribution during this period was the study of *Doberitz* [1968], who used cross-spectrum analysis to quantify relationships between SST, surface wind, and rainfall at island stations in the equatorial dry zone of the central and eastern equatorial Pacific.

2.2. Bjerknes' [1969] Synthesis

Television pictures from weather satellites launched during the 1960s provided a more comprehensive view of the evolving seasonal-mean cloud and rainfall fields over the equatorial Pacific during the continuing sequence of large-amplitude swings of the SO and the related El Niño phenomenon, setting the stage for the seminal ENSO synthesis of *Bjerknes* [1969]. Integrating the new information from satellites with conventional surface and upper-air observations from Canton Island in the context of earlier studies dating back to those of *Walker* [1924], Bjerknes identified coupled ocean-atmosphere interactions in the equatorial Pacific as the source of ENSO-related climate variability. In his comprehensive description of these interactions the central climatic feature is the east-west SST gradient between the pronounced dry zone over the cold waters of the eastern equatorial Pacific and the heavy convective rainfall over the warmer waters to the west. Bjerknes viewed the equatorial easterlies that link these areas of sinking and rising air as the lower branch of an east-west equatorial "Walker Circulation," driven by the basin-scale SST gradient. He proposed that variations in the Walker Circulation couple the circulation field of Walker's SO to the zonal gradient of SST in the equatorial Pacific. While the regional El Niño phenomenon of the eastern equatorial Pacific remains part of the picture in his explanation, the central feature is the basin-scale oscillation in SST that forces the planetary-scale circulation anomalies associated with the SO.

Bjerknes [1969, p. 170] characterized the feedback process between ocean and atmosphere as follows:

> A change toward a steeper pressure slope at the base of the Walker Circulation is associated with an increase in the equatorial easterly winds and hence also with an increase in the upwelling and a sharpening of the contrast of surface temperature between the eastern and western equatorial Pacific. This chain reaction shows that an intensifying Walker Circulation also provides for an increase of the east-west temperature contrast that is the cause of the Walker Circulation in the first place. On the other hand, a case can also be made for a trend of decreasing speed of the Walker Circulation....

While the notion of a positive feedback between SST and atmospheric circulation seemed well supported by the evidence, the fundamental question of how the coupled system evolves from the warm state to the cold state and vice versa remained to be answered. In the words of *Bjerknes* [1969, p. 170]: "There is thus ample reason for a never-ending succession of alternating trends by air-sea interaction in the equatorial belt, but just how the turnabouts between trends takes place is not quite clear." Answering this question required overcoming two major obstacles. The first was the primitive understanding of equatorial ocean dynamics that existed at that time, and this contributed to the second, the lack of a coupled modeling capability. With only a few exceptions, e.g., *McWilliams and Gent* [1978], theoretical and modeling studies prior to TOGA primarily focused on the two simpler "uncoupled" questions: (1) What is the equatorial Pacific Ocean response to anomalous wind forcing? and (2) What is the global atmospheric response to equatorial Pacific SST anomalies? The question of why the coupled system oscillates remained for TOGA to address.

2.3. The Canonical El Niño

Bjerknes' [1969] synthesis stimulated numerous observational studies, which, by the early 1980s, provided a much improved description of the structure and evolution of ENSO. Some of these studies contributed to a better description of its structure and spatial extent; e.g., *Trenberth* [1976], *Weare et al.* [1976], *Wright* [1977], *Quinn et al.* [1978], *van Loon and Madden* [1981], and *Pazan and Meyers* [1982]. Others were more focused on the evolution of the tropical Pacific warm phase anomaly fields, e.g., *Wooster and Guillen* [1974], *Ramage and Hori* [1981], and *Weare* [1982]. A description of the typical evolution of the warm phase anomaly fields emerged from these studies, which was referred to by *Cane* [1983] as the "canonical El Niño". Particularly influential in this development were the papers of *Wyrtki* [1975] and *Rasmusson and Carpenter* [1982].

On the basis of a study of the evolution of the equatorial wind and sea level fields during the 1957–1958, 1965, and 1972–1973 warm episodes, *Wyrtki* [1975] concluded that El Niño warmings along the South American coast are not the result of local changes in surface wind forcing (i.e., decreased upwelling), as previously thought, but rather reflect a remote SST response to a rapid decrease in the easterlies in the equatorial central Pacific. He described a sequence of events culminating in the onset of a coastal warming. It begins with a "buildup phase" of abnormally strong equatorial easterlies, during which the slope of the sea level and the thermocline across the equatorial Pacific increases, as warm water accumulates on the western side of the basin. The termination of this regime is marked by a rapid collapse of the easterlies, which remained unexplained since *Wyrtki* [1975] was not addressing the coupled problem. The rapid decrease in the easterly wind stress excites an equatorial Kelvin wave,

characterized by an eastward surge of warm surface water. With the arrival of the Kelvin wave in the eastern Pacific, the thermocline is depressed, and rapid warming ensues. Later studies [e.g., *Barber and Chavez*, 1983; *McPhaden and Picaut*, 1990] showed that the intensity of the upwelling during the warming is little changed, but the upwelled water is warmer, since it now originates from above rather than below the deeper thermocline.

Wyrtki's [1975] scenario addressed the question of the onset of the coastal El Niño warming from the standpoint of the forcing of the ocean by an abrupt change in zonal wind stress, rather than the more slowly evolving basin-scale warming of the coupled system envisioned by *Bjerknes* [1969]. His study had significant implications for prediction of the coastal warming; that is, it would follow a precursor buildup phase, and there would be a roughly 2-month lag between the collapse of the easterlies and the arrival of the Kelvin wave at the coast. Simple ocean model simulations [*Hurlburt et al.*, 1976; *McCreary*, 1976; *Busalacchi and O'Brien*, 1981] and a subsequent analysis of the 1976 warming [*Wyrtki*, 1979] provided further evidence in support of this scenario.

Since the coastal El Niño warmings are associated, even in the Spanish name, with a particular season, there is reason to believe that the general pattern of ENSO-related anomalies may be constrained by the evolving annual march. With this in mind, *Rasmusson and Carpenter* [1982, hereinafter referred to as RC] described the mean seasonal pattern of the warm episode wind, SST, and rainfall anomaly fields in terms of seasonal composites, on the basis of six major warm episodes that occurred between 1950 and 1976.

The warm episode composites suggested a fairly systematic evolution, which had the implication that the evolving pattern might be predictable once the episode is underway. In agreement with *Wyrtki's* [1975] study the RC composite warm episodes showed stronger than normal equatorial easterlies to the west of the date line during the months preceding the onset of the warm episode. The easterly anomalies were replaced by westerly anomalies in the western Pacific during October-November of the year prior to the warming, accompanied by the appearance of positive equatorial SST anomalies near the date line. Larger positive SST anomalies developed in the eastern equatorial Pacific early in the following year, reaching maximum values around April-June. Positive SST anomalies expanded westward from the coast into the central equatorial Pacific in subsequent months, and the westerly wind anomalies in the central equatorial Pacific intensified, becoming most strongly developed during August-December. During the following northern winter (December-February), which RC referred to as the "mature phase" of the warming, the positive SST and rainfall anomalies were concentrated in the central equatorial Pacific, and the lower branch of the equatorially symmetric "Hadley Circulation" was intensified in this sector, contributing to increased low-level convergence in the equatorial belt. The mature phase was followed, a season later, by a decay in the anomaly patterns and their replacement by a developing pattern of cold phase anomalies. *Barnett's* [1983] analysis of maritime surface observations over the Pacific and Indian Oceans, based on complex empirical orthogonal function analysis, confirmed the sequence of evolution described above.

By 1982 the canonical El Niño was widely accepted as a reliable description of the sequence of events associated with a warm episode of what is sometimes termed the "ENSO cycle." Confidence in this conceptual model engendered an air of optimism regarding the prediction of the onset and evolution, if not the amplitude, of warm episodes. This optimism was rudely dashed by the 1982–1983 warm episode.

2.4. Lessons From the 1982-1983 Warm Episode

The strong reliance on the canonical precursors and a subsequent evolution that is phase locked to the annual march resulted in a significant delay in recognizing the 1982–1983 episode for what it was. The observations available at that time, i.e., SLP, in situ SST, sea level height, surface and upper air wind analyses, and outgoing longwave radiation (OLR, an indicator of deep convective cloudiness), were adequate to define the large-scale features of the developing anomaly fields. By August 1982 many of the characteristic features of warm episodes of the ENSO cycle were already in evidence. However, for lack of a significant buildup phase and because the warming propagated eastward across the basin from the central Pacific, rather than westward from the South American coast, the research community was caught off guard. Erroneous satellite-derived SST estimates, which were contaminated by the El Chichon volcanic eruption, also contributed to the failed characterization of the tropical climate state [*McPhaden et al.*, this issue]. In retrospect it seems clear that the delay in recognizing the developing 1982–1983 warm episode was primarily due to a flawed conceptual framework rather than to the inadequacy of the observations.

The marked departure of the 1982–1983 warm episode from the RC canonical evolution based on analysis of the six prior major warm episodes raised a number of new questions. The post mortem modeling and diagnostic studies that followed set the stage for the TOGA program. The magnitude of the 1982–1983 warm episode was of historical proportions, but how atypical was its evolution? Regarding the lack of a precursor buildup phase, an extended period of above-normal equatorial easterlies corresponds to a high index state of the SO, which is identified with the cold phase of the ENSO cycle. Examination of more extended time series of indices of the SO and equatorial Pacific SST indicates that not all significant warm episodes have been preceded by pronounced cold phases; for example, *Rasmusson and Wallace* [1983] noted that the evolution of the 1940–1941 warm episode, which predated the episodes used in the RC composite, was similar in many respects to the 1982–1983 episode. Although the evolution of the 1982–1983 warm episode did not conform to the RC composite, the seasonality of the Peru coast anomaly time series was generally similar. For example, the largest SST anomalies along the coast occurred early in the calendar year, as in prior events, but in contrast to the composite, this El Niño event occurred toward the end, rather than at the onset, of the basin-wide warm episode.

On the eve of the TOGA program, the canonical picture was being reevaluated, and there was an increased diagnostic emphasis on the variations in the western Pacific warm pool. A new set of questions was emerging which included the event-to-event consistency and secular variability of the ENSO phenomenon.

3. ENSO Variability During TOGA

The ENSO phenomenon exhibited a variety of behavior during the 10-year lifetime of the program 1985–1994, as evidenced by the extended time series of the SST "cold tongue index" shown in Plate 1. The record-breaking 1982–1983

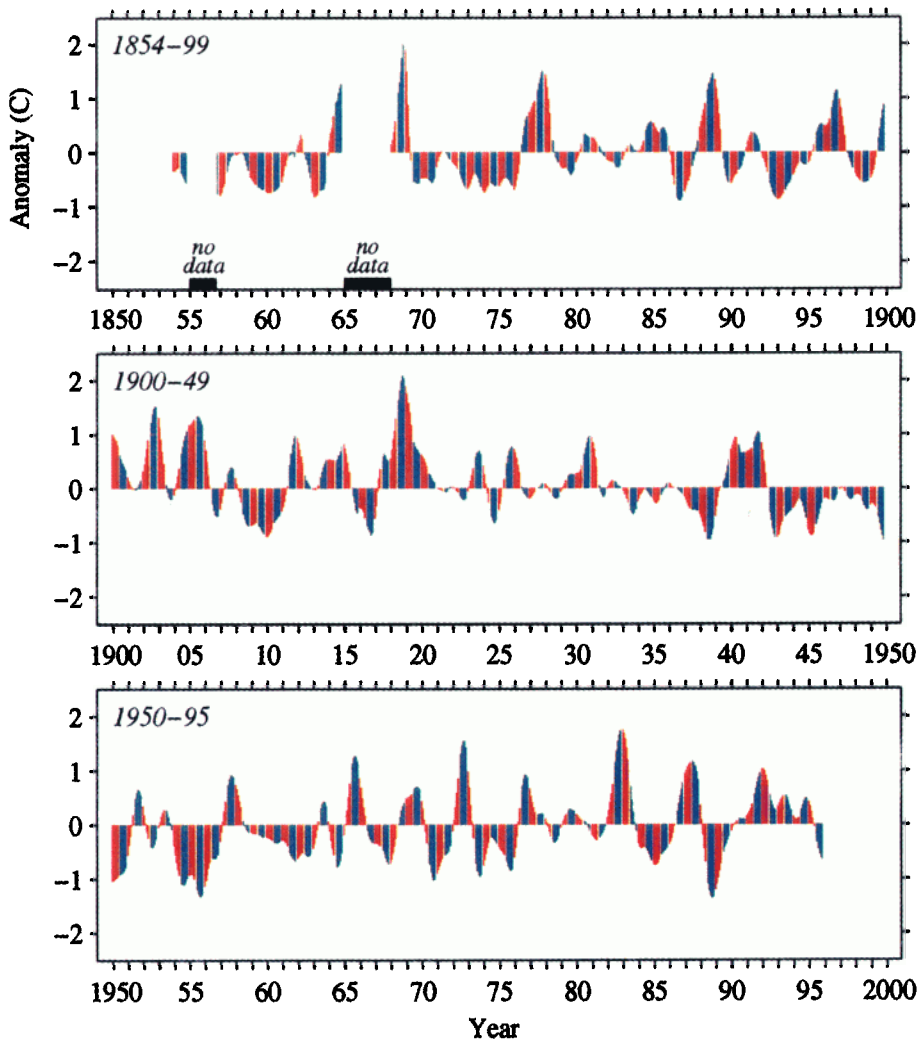

Plate 1. Monthly mean sea surface temperature (SST) anomalies (degrees Celsius) averaged over the central and eastern equatorial Pacific (6°N–6°S, 180°–90°W). Anomalies are with respect to the entire record. Successive nine- and five-point running mean filters have been applied to the time series. January–May (July–November) values are indicated by red (blue) shading. SST values for 1854–1992 were obtained from the Comprehensive Ocean-Atmosphere Data Set (COADS) [*Woodruff et al.*, 1987, 1993] and for 1993–1995 from NOAA/NCEP [*Reynolds and Smith*, 1994].

warm episode was followed by another well-defined warm episode that set in around August 1986 and lasted into early 1988 and by a more prolonged warm period that spanned much of the early 1990s and exhibited several minor peaks. By some measures the interval extending from April 1988 to mid-1989 was as cold in the equatorial Pacific as any period of comparable length since the mid-1950s. Compared to the previous 35 years, the ENSO cycle from the late 1970s onward (including the TOGA decade) has exhibited less of a tendency for phase locking with the annual cycle (with peaks coinciding with the "cold season" July-November indicated by the blue-shaded bands in Plate 1) and less of a tendency for a quasi-biennial rhythm [*Barnett*, 1983; *Rasmusson et al.*, 1990] than is apparent in segments of the 1950–1976 record. *Trenberth and Shea* [1987] noted an analogous lack of stationarity with respect to the regularity of the ENSO cycle in earlier segments of the record.

Descriptions based on a single index do not do justice to the complexity of the climate variability over the equatorial Pacific during the TOGA decade. Plate 2 shows time series of the three SST indices defined by RC, together with the conventional Southern Oscillation Index (SOI). Niño 1+2 represents conditions off the Peru coast; Niño 3 is an equatorial strip extending from 90° to 150°W; and Niño 4 is an equatorial strip centered on the date line. The SOI is the normalized difference between normalized SLP differences, Tahiti minus Darwin. The major warm and cold episodes of the ENSO cycle are evident in all four series, but the correspondence between the amplitude and the timing of individual episodes is far from perfect. For example, the 1982–1983 warm episode was much more prominent and persisted longer in Niño 1+2 than in Niño 4. The contrasts in the behavior of the indices are particularly notable during the second half of the TOGA decade (1990-1994), when Niño 1+2 averaged only slightly above normal and exhibited a sequence of short-lived warm and cold episodes, while Niño 4 exhibited what appeared to be a single, virtually uninterrupted warm episode, most of which is mirrored in the SOI. In the following

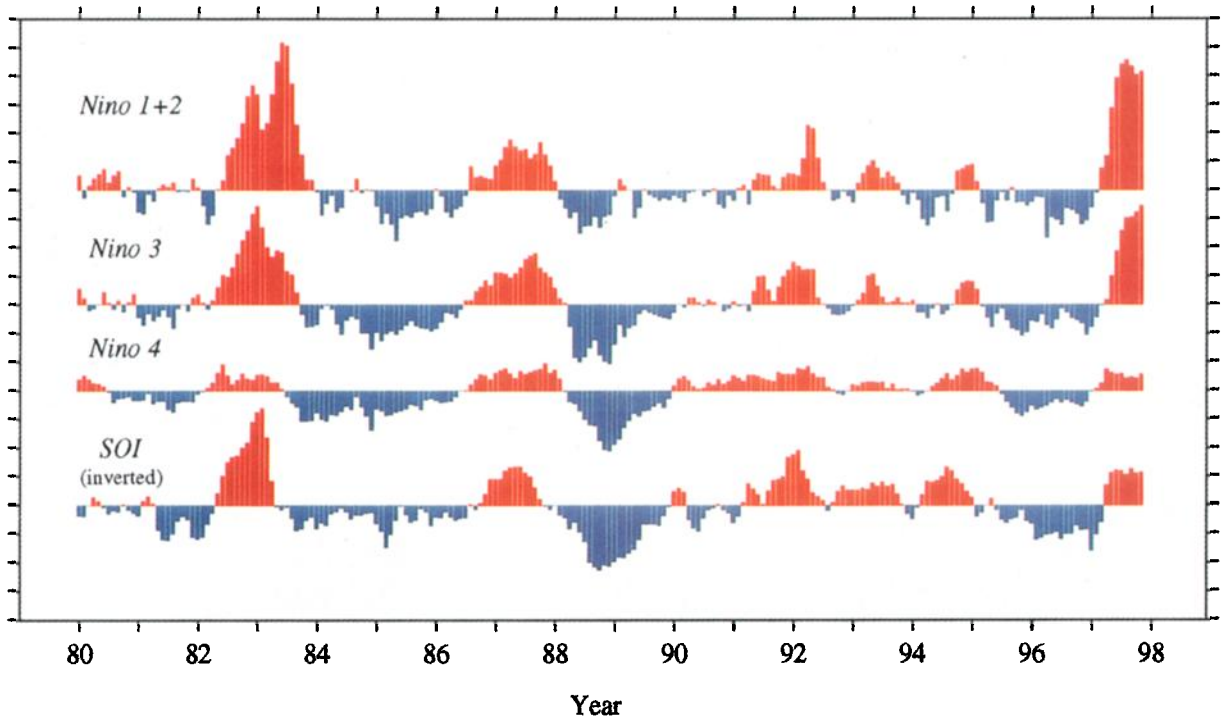

Plate 2. Monthly mean SST anomalies averaged over the Niño 1+2 (0°–10°S, 90°–80°W), Niño 3 (5°N–5°S, 150°–90°W), and Niño 4 (5°N–5°S, 160°E–150°W) regions together with the conventional Southern Oscillation Index (SOI) (the normalized difference between normalized sea level pressure (SLP), Tahiti minus Darwin). Each ordinate tick mark represents 1°C for the SST indices and one standard deviation of the SOI. Anomalies in this and subsequent plates are with respect to the TOGA decade, 1985–1994. Indices are from the NOAA/NCEP Climate Prediction Center.

subsections we will consider separately the year-to-year variability of the ENSO cycle during the TOGA decade and the variations in the mean state of the tropical Pacific from the first to the second half of the TOGA decade.

3.1. Interannual Variability

The variability of SST within the equatorial Pacific waveguide (4°S–4°N) during the TOGA decade is displayed in a time versus longitude format in Plate 3b. The first 5-year period (1985–1989) was dominated by swings from cold to warm and back to cold again in association with the onset and cessation of the 1986–1987 warm episode and the 1988–1989 cold episode that immediately followed, both of which rank among the major features in the 142-year-long historical record shown in Plate 1.

Consistent with the RC composite, the warm episode along the South American coast in 1987 peaked early in the calendar year, about 6 months in advance of the strongest basin-wide SST anomalies (Plates 2 and 3). However, in contrast to the prevailing interpretation of the canonical El Niño [e.g., *Cane*, 1983], the SST anomalies did not spread westward from the South American coast to the interior of the basin. Rather, it seems that the basin-wide anomalies developed in situ while the coastal anomalies weakened. The lack of time continuity between these features is consistent with the results of *Trenberth and Shea* [1987], *Deser and Wallace* [1987], *Wright et al.* [1988], and *Trenberth and Hoar* [1996], which indicate that the coastal SST perturbations documented by *Quinn et al.* [1978] in reference to El Niño and the basin-wide SST perturbations that *Bjerknes* [1969] linked to the major swings of the SO are only weakly coupled.

Higher-frequency variability is clearly evident in Plate 3, superimposed upon the major swings of the ENSO cycle. For example, the 1988–1989 cold episode was marked by two distinct extrema, which are also evident in Plate 2; the first in the eastern part of the basin around May 1988 and the second centered near the date line about 6 months later. Weaker changes of opposite polarity were observed at the western end of the basin.

Consistent with Plate 2, the variability during the second half of the TOGA decade (1990–1994) was somewhat different in character from that observed during the first half. Strong positive SST anomalies in the vicinity of the date line prevailed throughout virtually the entire period, while farther to the east, SST exhibited weak, irregular fluctuations with a characteristic period of the order of a year. There were times during the second half of TOGA when SST was well above normal near the date line but near or below normal along the South American coast. Relatively short-lived warm episodes peaked in mid-1991, early 1992 and 1993, and late 1994, of which the 1992 episode was the most prominent. Like the 1986–1987 warm episode, the 1992 and 1993 episodes were accompanied by negative SST anomalies at the western end of the basin and westerly equatorial wind stress anomalies (indicated by the vectors in Plate 3).

Plate 3a shows the corresponding time-longitude section of the anomalies in the depth of the 20°C isotherm along the equator, an indicator of displacements in the thermocline depth, obtained from the data assimilation system of the

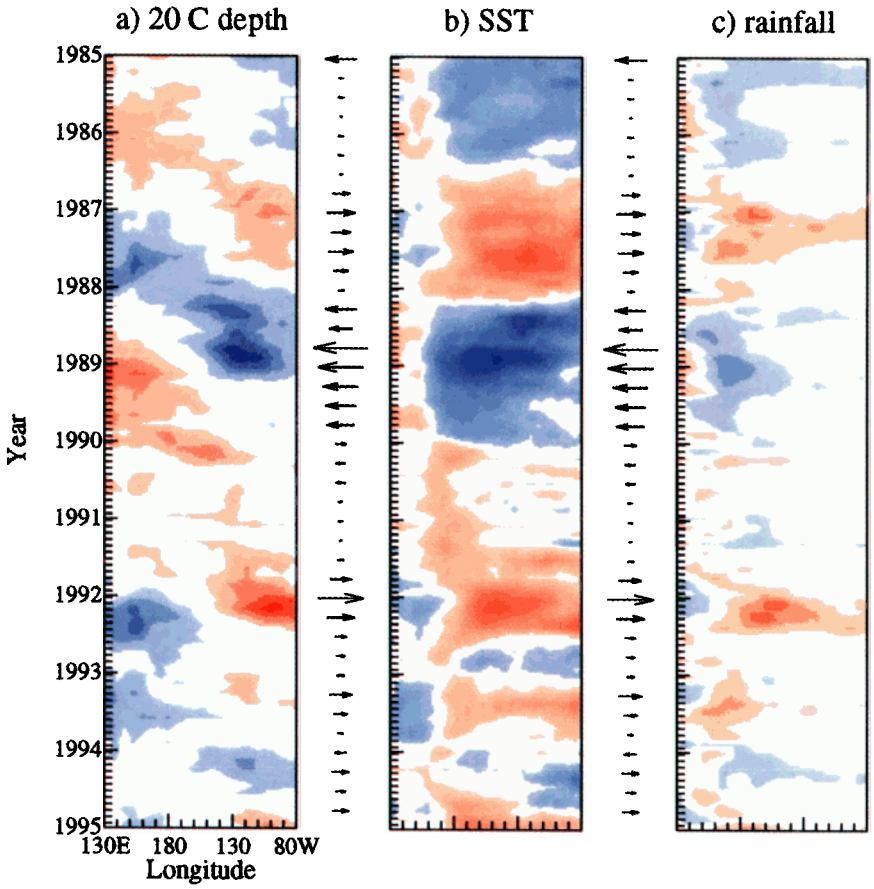

Plate 3. Time-longitude diagram of anomalies in the equatorial Pacific for (a) 20°C isotherm depth (4.5°N–4.5°S), (b) SST (4°N–4°S), and (c) rainfall (5°N–5°S) for the TOGA decade starting January 1, 1995. Arrows represent area-average zonal pseudostress over 4°N–4°S, 151°E–141°W. Positive (negative) values are indicated by red (blue) shading. Lightest (saturated) shading denotes isotherm depth, SST, and rainfall anomalies > 10 m, 0.25°C, and 5 cm month^{-1} (40 m, 2°C, and 25 cm month^{-1}) in magnitude, respectively. The largest magnitude zonal stress anomaly is −24 m^2 s^{-2}. Isotherm depths are taken from the ocean data assimilation model at NOAA/NCEP; pseudostress from Florida State University [*Stricherz et al.*, 1992]; SST from NOAA/NCEP [*Reynolds and Smith*, 1994], and microwave sounding unit (MSU) rainfall from the NASA/Marshall Space Flight Center [*Spencer*, 1993].

National Oceanographic and Atmospheric Administration (NOAA)/National Centers for Environmental Prediction (NCEP) model. As documented by *McPhaden et al.* [this issue], these displacements are largely a reflection of the response of the ocean model to variations in equatorial wind stress. In the eastern half of the basin they closely match the SST anomalies, even with respect to the minor features pointed out above. There also appears to be a rough correspondence between the SST and thermocline displacement anomalies at the western end of the basin. For reasons that are not clear to us the major displacements exhibited a preference for eastward phase propagation during the TOGA decade, with individual features crossing the Pacific basin in about a year, whereas the SST anomalies exhibited no such preference. Conversely, the distinct suggestion of a nodal line along 160°E in the SST anomaly pattern is not evident in the thermocline displacement.

The major advances in satellite monitoring of tropical rainfall during the TOGA decade have revealed the full extent of the correspondence between rainfall and the strength of the trade winds in the equatorial belt, first pointed out by *Brooks and Braby* [1921]. The distribution of equatorial (5°N–5°S) rainfall anomalies as inferred from microwave sounding unit (MSU) imagery using the algorithm developed by *Spencer* [1993] is shown in Plate 3c. As documented in the appendix, the features in this analysis are generally consistent with rainfall estimates from the special sensor microwave/imager (SSM/I) [*Ferraro et al.*, 1996], with the GOES precipitation index (GPI) on high-resolution infrared satellite imagery [*Joyce and Arkin*, 1997], and with the rainfall estimates based on a blend of in situ and satellite measurements and numerical weather prediction model output [*Xie and Arkin*, 1996]. In general, the rainfall anomalies match the SST anomalies remarkably well, even with respect to the high-frequency fluctuations. In agreement with many previous studies the zonal structure of the two fields is somewhat different; the node in the rainfall anomaly pattern is about 15° to the west of the node in the SST anomaly pattern and the stronger rainfall anomalies tend to be somewhat more concentrated in the central Pacific (but not nearly as much so as in the corresponding OLR section shown in Plate A1a).

Plate 4 is the counterpart of Plate 3 for the total fields, including the seasonally varying climatological means. The annual march dominates the SST variability in the equatorial

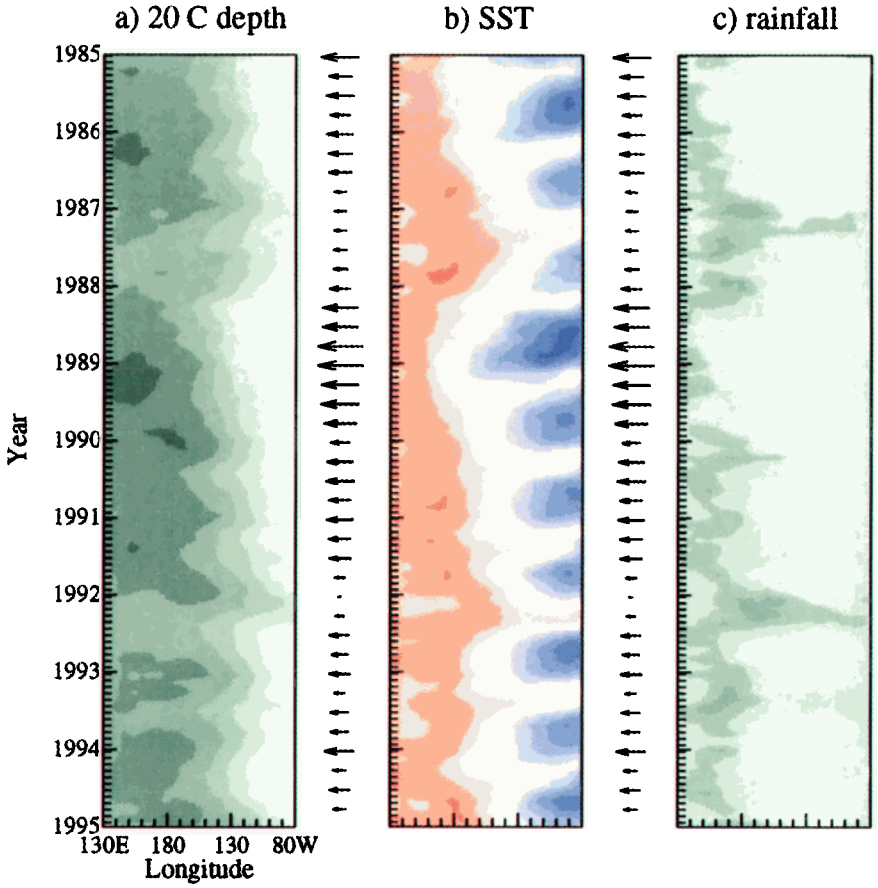

Plate 4. As in Plate 3, but for total fields. Progressively darker shading is for 20°C isotherm depths > 60, 90, ..., 180 m and rainfall amounts > 5, 20, 35 cm month^{-1}. SSTs < 26°, 25°, ... 22°C (>28°, 29°, 30°C) indicated by blue (red) shading with progressively greater saturation. The largest magnitude zonal pseudostress is –45 m^2 s^{-2}.

eastern Pacific. In contrast to the SST anomalies shown in Plate 3, the SST perturbations associated with the annual march propagate westward from the South American coast to the date line over a period of several months, as shown previously by *Wyrtki* [1965] and *Horel* [1982]. Near the coast an El Niño event can be viewed as an enhancement of the climatological mean warm season [*Wyrtki*, 1975], as manifested in the pink strips extending westward from the coast in the early months of 1987, 1992, and 1993. Farther to the west, where the annual march is rather weak and there exists a strong year-round east-to-west SST gradient, the zonal excursions of the isotherms resemble the Niño 4 temperature plot in Plate 2; warm episodes correspond to an eastward expansion of the "warm pool," delineated by the 28° or 29°C isotherm [*McPhaden and Picaut,* 1990; *Picaut et al.,* 1996].

East of the date line, the section for the rainfall, shown in Plate 4c, exhibits a strong annual march with a distinct wet season that closely parallels the warm season in the SST section, including the westward propagation. Years with warmer than normal warm seasons tend to be characterized by strong and/or abnormally long rainy seasons. Farther to the west, the annual march is less pronounced. During warm episodes the zone of year-round heavy rainfall over the western Pacific expands eastward with the warm pool, bringing with it an increase in rainfall, even during the dry season.

Plate 5b shows the zonally averaged SST anomalies in the tropical Pacific from the date line eastward in a time-latitude format, dating back to mid-1981. This mode of presentation distinguishes more clearly between the higher-frequency fluctuations with periods of the order of a year, which tend to be largely restricted to the equatorial zone and the lower-frequency variability, which tends to be relatively more prominent off the equator. The equatorial symmetry in this plate is quite striking. The characteristic bowed shape of many of the contours is indicative of the tendency for SST perturbations on the equator to lead those off the equator, consistent with the notion that SST within ~10° of the equator is strongly influenced by the time-varying volume and temperature of the water upwelled within 1° of the equator. The narrowness of the upwelling zone relative to the cold tongue is evident in the signature of the phytoplankton in high-resolution coastal zone color scanner satellite imagery and in the mean meridional motions of drifting buoys [*Poulain,* 1993]. The associated off-equatorial meridional wind anomalies characteristic of the mature phase of the RC composite are also clearly evident. Time series of equatorial SST and zonal pseudostress, shown in Plate 5c, indicate that warm episodes coincide with westerly wind anomalies along the equatorial western and central Pacific and vice versa. The corresponding zonally averaged rainfall anomalies, shown in Plate 5a, exhibit a less clearly defined meridional structure and some tendency for the largest anomalies to be biased toward the north of the equator, toward the climatological-mean Intertropical Convergence Zone (ITCZ). These differences

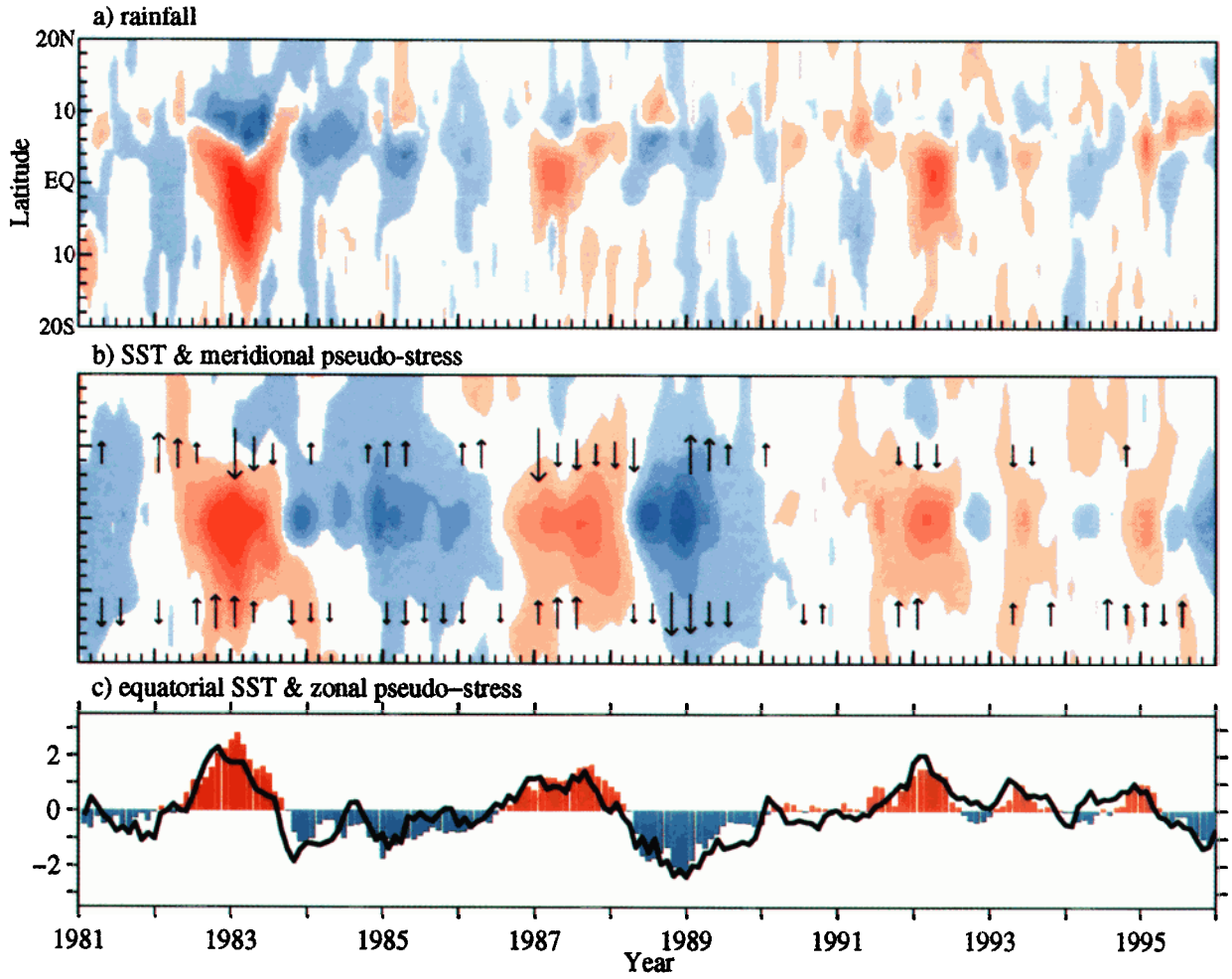

Plate 5. Time-latitude diagram of zonal mean (180°–90°W) anomalies in (a) rainfall and (b) SST and meridional pseudostress; and (c) equatorial (4°N–4°S) SST and zonal pseudostress anomalies averaged over 180°–90°W and 151°E–141°W, respectively. In plates (a) and (b), monthly mean rainfall and SST means are centered at 1.25°, 3.75°, ..., 18.75° and 1°, 3°, ..., 19° latitude in each hemisphere, respectively. Positive and negative values are shaded red and blue, respectively. Zonal mean rainfall anomalies > 2.5 cm month^{-1} in magnitude shaded with anomalies ranging from < –17 to > 22 cm month^{-1}. Zonal mean SST anomalies > 0.25°C in magnitude shaded with values ranging from < –1.75° to > 1.25°C. Seasonal mean indices of coherent meridional pseudostress anomalies to the north and south of the equator (16°–2°N, 151°E–141°W, and 6°–20°S, 151°E–141°W, respectively) are plotted in vector format at their respective central latitudes (maximum vector magnitude plotted is 15 m^2 s^{-2}). In plate (c), equatorial SST (degrees Celsius) and zonal pseudostress anomalies (in tens of m^2 s^{-2}) are depicted by shading and a contour, respectively. Pseudostress and MSU rainfall data sources are as in Plate 3; SST values from NOAA/NCEP for 1981 are from *Smith et al.* [1996], values for 1982–1995 are from *Reynolds and Smith* [1994].

notwithstanding, the timing of the anomalies agrees quite well with those in SST.

Plate 6 is the counterpart of Plate 5 for the total fields of rainfall and SST, including the seasonally varying climatological means. In the annual mean the ITCZ in the rainfall pattern coincides with the warmest water along 10°N, and the equatorial dry zone coincides with the cold tongue in the SST. A weak southern hemisphere ITCZ makes a brief appearance along 7°S in February-March of the warmer years; it is apparent in the MSU, SSM/I, and GPI rainfall climatologies, distinct from the South Pacific Convergence Zone farther to the west. Heavy rainfall never intrudes into the equatorial dry zone during the cold season, but during the warm seasons of the stronger warm episodes the dry zone was virtually obliterated. The correspondence between the SST and rainfall distributions is quite striking: even the irregularities from one year to the next match quite well.

Plates 7 and 8 provide an overview of the global anomaly patterns associated with the ENSO cycle during the first 9 years of the TOGA decade. They were constructed by regressing the global fields listed in the plate captions upon the time series of cold tongue SST in Plate 1. The patterns and their amplitudes are representative of conditions observed during the warm phase of a weak swing of the ENSO cycle. Plate 7 is based entirely upon observed fields, while Plate 8 contains model-derived fields from the NCEP/National Center for Atmospheric Research (NCAR) reanalysis project [*Kalnay et al.*, 1996], which along with similar National Aeronautics and

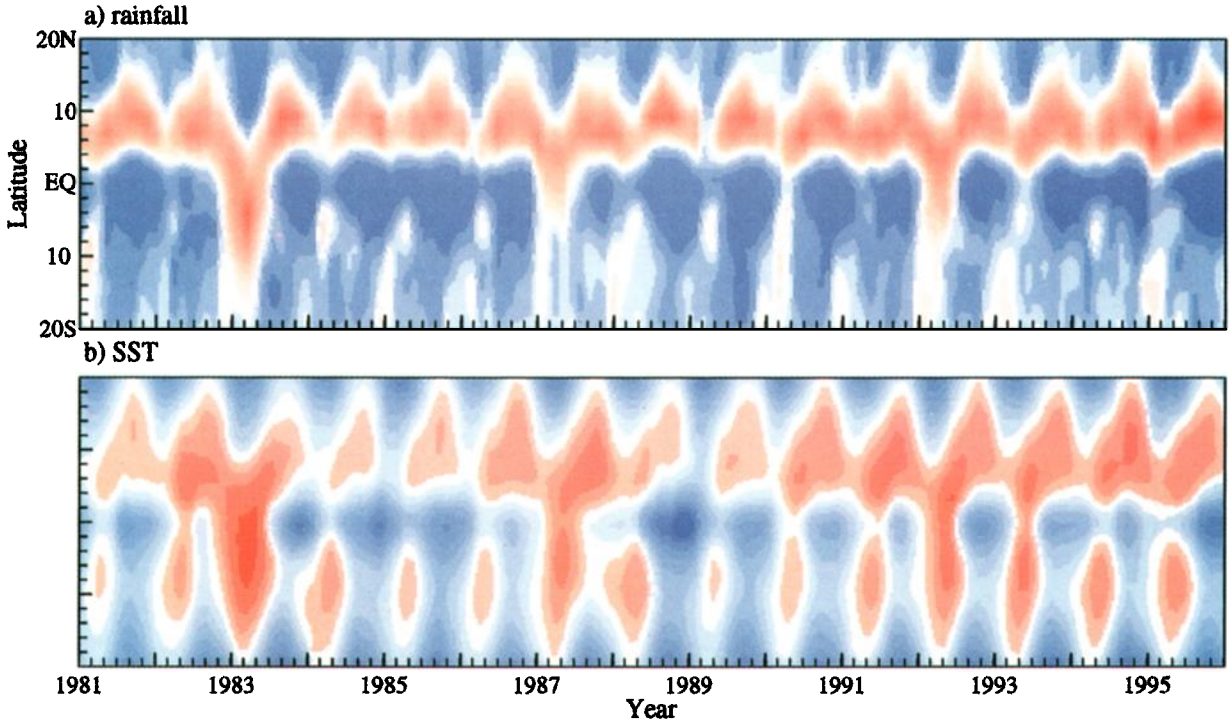

Plate 6. As in Plates 5a and 5b, but for total fields. Zonal mean rainfall interval of 2.5 cm month^{-1} in magnitude is shown with values ranging from < 2.5 (blue) to 10 (white) to > 50 cm month^{-1} (red). Zonal mean SST interval of 0.5°C with values ranging from < 23° (blue) to 27° (white) to > 29°C (red).

Space Administration (NASA) [*Schubert et al.*, 1993] and European Centre for Medium-Range Weather Forecasts (ECMWF) [*Gibson et al.*, 1997] efforts, were set in motion during the TOGA period [*Bengtsson and Shukla*, 1988] and are now nearing completion.

Observed SST and surface wind anomalies shown in Plate 7c strongly resemble the patterns in the RC warm episode composite and the leading nonseasonal empirical orthogonal function (EOF) of Pacific SST of *Weare et al.* [1976], both of which are based on pre-TOGA data. The winds derived from the reanalysis (Plate 8) capture the major features of the observed winds except for the patch of southerly anomalies in the equatorial eastern Pacific, which may be a shallow boundary-layer feature, unrelated to the SLP field [*Wallace et al.*, 1989]. A distinctive SO signature reminiscent of *Trenberth and Shea* [1987, Figure 1] is evident in the SLP anomalies shown in Plates 7b and 8b. The resemblance is even stronger if correlation coefficients are plotted instead of regression coefficients (not shown). The reanalyzed pressure field captures the spatially coherent structures inherent in the COADS data. The MSU rainfall anomalies are not quite as well replicated in the reanalysis: instead of being broadly distributed throughout the outer part of the climatological mean equatorial dry zone, they tend to be somewhat more concentrated along the equator near 160°W. The band of enhanced rainfall along the northern periphery of the dry zone in the satellite observations ties in well with the enhanced rainfall observed over the Galapagos Islands and along the coast of Ecuador and northern Peru during El Niño, whereas the corresponding feature in the reanalysis intersects the coast farther north, near Panama. Despite these discrepancies, the agreement between the two rainfall patterns is quite impressive when viewed from a global perspective.

The corresponding pattern of tropospheric (1000-200 hPa layer mean) temperature anomalies, shown in Plates 7a and 8a is dominated by the same distinctive "dumbbell pattern" in the tropical eastern Pacific that is apparent in the results of *Yulaeva and Wallace* [1994], based on the partially overlapping period of record 1979-1991, which includes the 1982-1983 event. The wave pattern in the equatorial belt is reminiscent of theoretical solutions of *Matsuno* [1966], *Webster* [1972], and *Gill* [1980]. Other features of interest are the prevalence of positive anomalies throughout the entire tropics and the enhanced baroclinity along 30°N and 30°S over much of the Pacific and the Americas. The reanalysis captures the pattern in the satellite data extremely well, except for the relative minimum in the equatorial western Pacific.

With the addition of the TOGA decade the period of record is now sufficiently long so that the data can be stratified by season and by the warm/cold phase of the ENSO cycle. *Mitchell and Wallace* [1996] show that the rainfall anomalies associated with the warm phase of the ENSO cycle tend to be stronger and penetrate deeper into the core of the equatorial dry zone during the warm season December-May than during the cold season July-November. Presumably, during the cold season, SST in the interior of the dry zone remains below the 27°C threshold for deep convection [*Gadgil et al.*, 1984; *Graham and Barnett*, 1987], even during El Niño events. *Hoerling et al.* [1997] show that for similar reasons the SST and rainfall anomalies observed during the warm and cold phases of the ENSO cycle exhibit somewhat different spatial patterns. The warm phase is marked by a retreat of the cold

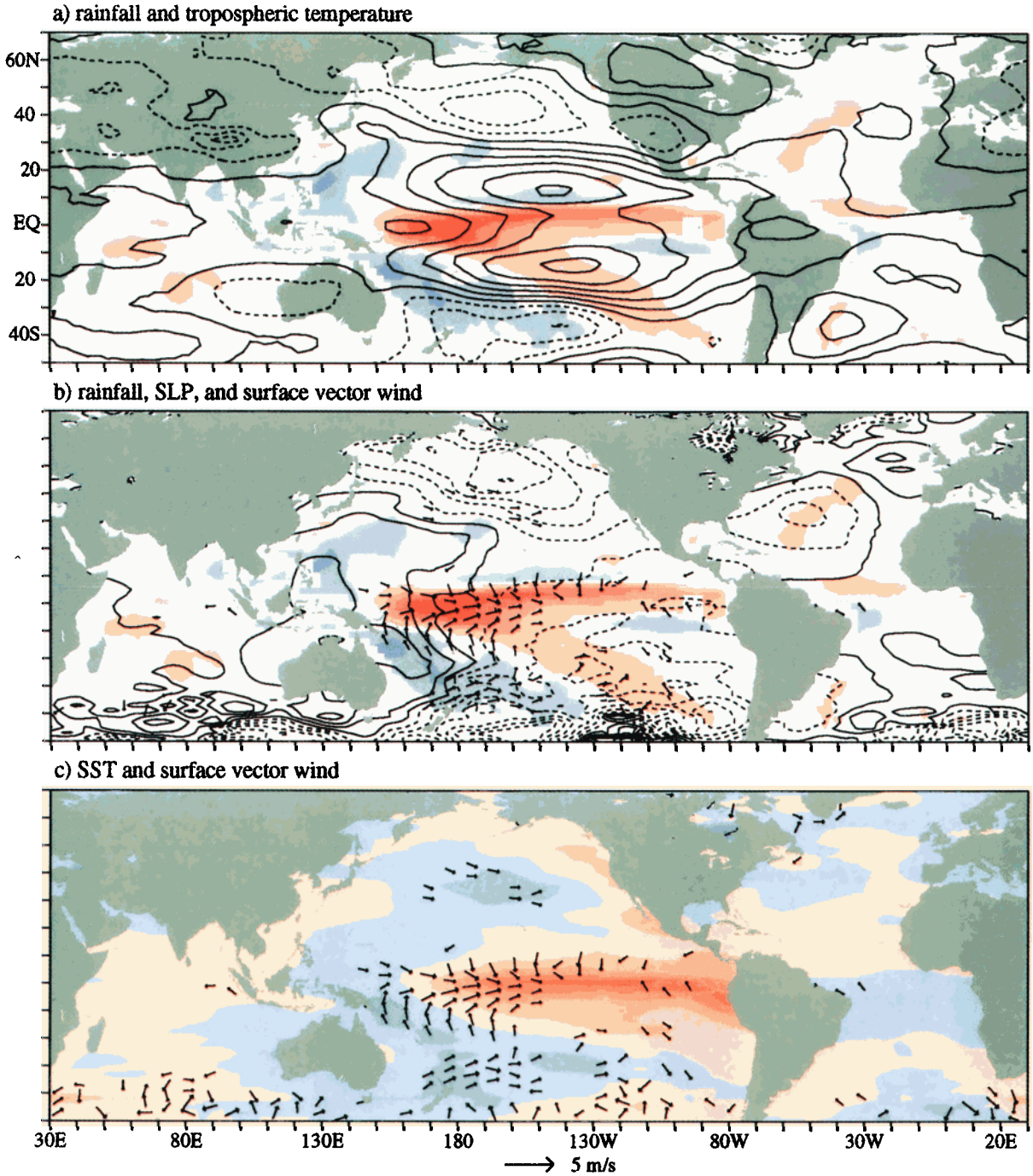

Plate 7. Selected fields regressed upon monthly values of the cold tongue index time series shown in Plate 1 for the period of record January 1985 through December 1993. All regression coefficients are per standard deviation of the cold tongue index. (a) Tropospheric layer mean temperature as deduced from channel 2 of the MSU (contour interval 0.1°C; negative contours are dashed) superimposed upon MSU rainfall (anomalies < -1 and -3 cm month^{-1} are shaded blue and > 1, 3, 5, and 7 cm month^{-1} are shaded red, with more saturated colors for larger magnitude anomalies). (b) SLP (contour interval 0.25 mbar, negative contours are dashed) superimposed upon rainfall as in plate (a). (c) Surface wind vectors superimposed upon SST. Only vectors > 0.5 m s^{-1} in magnitude are plotted; the SST anomaly shading interval is 0.25°C, with negative and positive anomalies shaded in blue and red, respectively. The SLP, surface vector wind, and SST were all obtained from COADS. MSU rainfall source as in Plate 3 and channel 2 temperature estimates are from *Spencer and Christy* [1990, 1992, 1993].

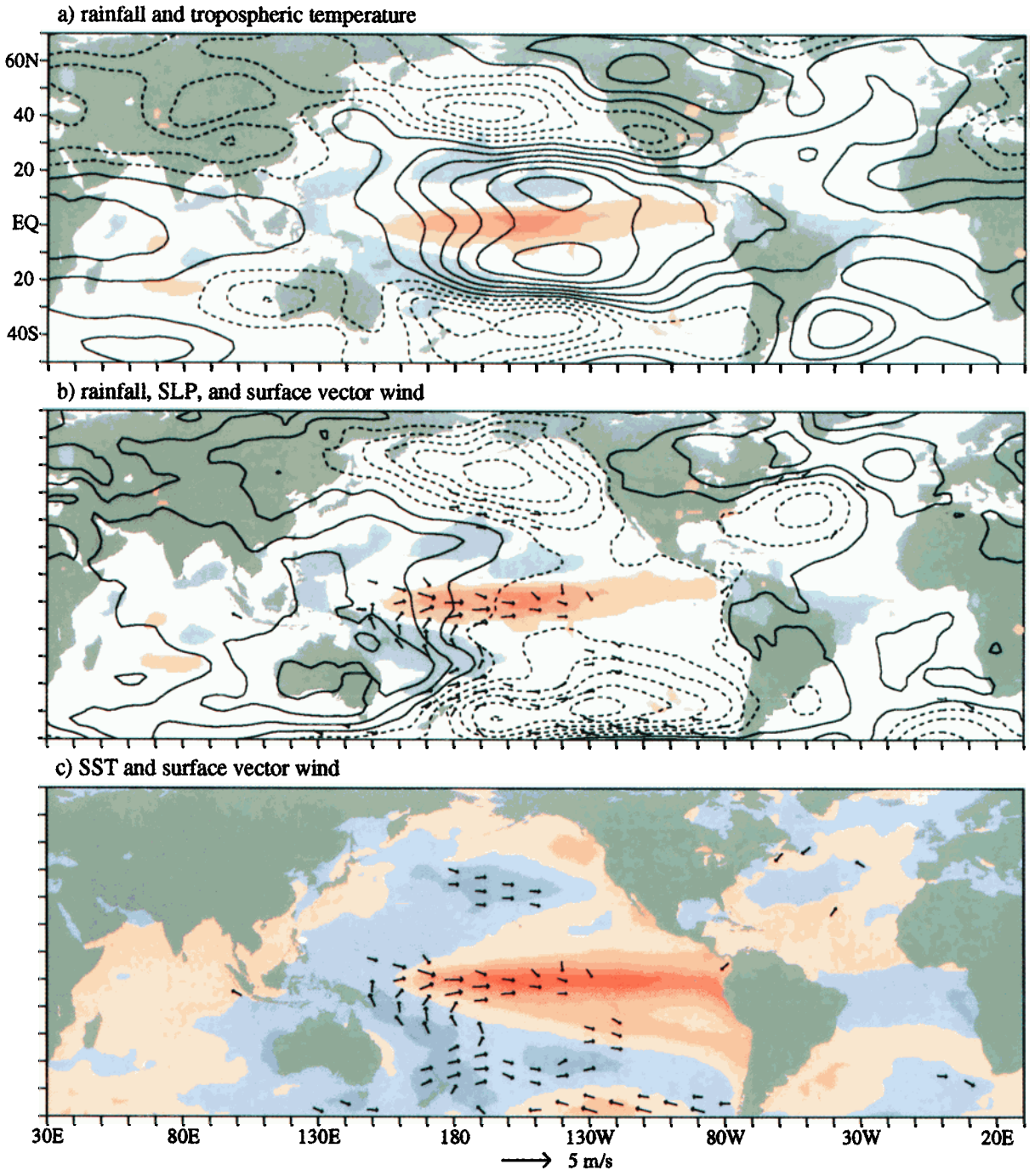

Plate 8. As in Plate 7, but for corresponding fields from the NCEP/NCAR reanalysis. (a) 1000-200 hPa layer mean temperature superimposed upon rainfall. (b) SLP and surface vector wind superimposed upon rainfall. (c) Surface vector wind superimposed upon SST from *Reynolds and Smith* [1994]. Shading and contouring conventions are as in Plate 7.

tongue and the equatorial dry zone into the eastern Pacific, and the cold phase is marked by a strengthening and westward expansion of the cold tongue and dry zone. Hence the anomaly patterns observed during the cold phase tend to be displaced westward relative to those observed during the warm phase, and *Hoerling et al.* [1997] demonstrate that this displacement has implications for the planetary-scale response to El Niño.

3.2. Longer-Term Variability

When viewed in the context of the entire 142-year time series in Plate 1, a striking characteristic of the TOGA decade is the overall warmth of the second half (1990–1994). Plate 9 shows the geographical distribution of the warming from 1985-1989 to 1990-1994, together with the corresponding changes in SLP, 850-hPa winds, and OLR. The changes are reminiscent of the differences in the respective fields between cold and warm episodes of the ENSO cycle on the interannual timescale, with pressure rises to the west of the date line and falls to the east, indicative of a drop in the SOI, a weakening of the easterlies along the equator, and an increase in rainfall in the equatorial central Pacific and farther to the east along the southern flank of the ITCZ.

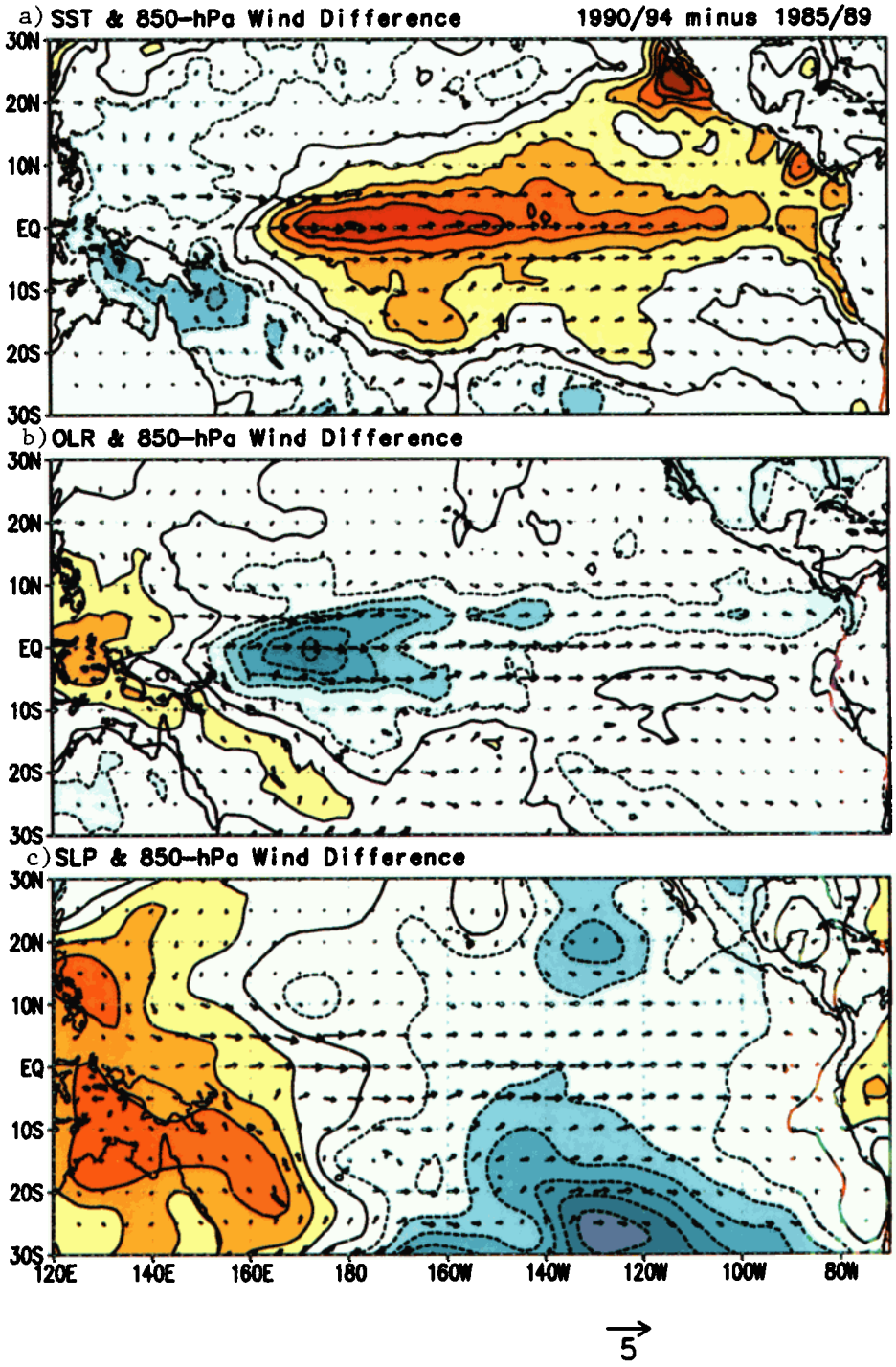

Plate 9. Change from 1985–1989 to 1990–1994 in mean (a) SST and 850-hPa vector wind, (b) outgoing longwave radiation (OLR) and 850-hPa vector wind, and (c) SLP and 850-hPa vector wind. Positive (negative) changes in scalar fields shaded red (blue), with the zero line indicated by a thick contour. SST, OLR, and SLP shading intervals are of 0.2°C, 4 W m^{-2}, and 0.2 hPa, respectively. Reference vector wind difference magnitude is 5 m s^{-1}. SST source is as in Plate 3; 850–hPa vector wind and SLP are from NCEP/NCAR reanalysis; and OLR is from NOAA/NCEP [*Chelliah and Arkin,* 1992].

Trenberth and Hoar [1996] noted that the prevalence of the warm polarity of the ENSO cycle throughout the second half of the TOGA decade is unprecedented in the 113-year record of a proxy SOI (Darwin SLP anomalies) that they examined and went on to speculate that this extraordinarily long warm episode might be indicative of a fundamental change in the character of the ENSO phenomenon, perhaps in response to the increase in global concentrations of greenhouse gases. The recurrence of the cold phase during 1995, which persisted for over a year (Plate 2) and the behavior of ENSO during the 1990s seem less extraordinary than it did 2 years ago. Nevertheless, the prevalence of the warm polarity of the ENSO cycle since 1977 seems to be continuing despite the tendency, pointed out by *Cane et al.* [1997], for warming on the 100-year

time scale to be less pronounced in the equatorial cold tongue region than for global SST as a whole.

The difference patterns in Plate 9 are unprecedented in terms of their clarity (owing to the quality of the SST analyses during TOGA) but not in terms of their large-scale structure; similar changes were observed for 5-year epochs 1977-1982 minus 1971-1976 [*Graham*, 1994], for the decades 1977-1986 minus 1967-1976 [*Nitta and Yamada*, 1989], and for the more extended epochs 1977-1993 minus 1950-1976 [*Zhang et al.*, 1997]. The SST pattern in Plate 9 also resembles the leading EOFs of low-pass-filtered Pacific and global SST [*Wang*, 1995; *Yukimoto et al.*, 1996; *Zhang et al.*, 1997]. The pattern is clearly "ENSO-like" in many respects, but in comparison to the interannual variability associated with the ENSO cycle, the SST anomalies are less equatorially trapped, particularly in the eastern Pacific. This rather subtle distinction shows up more clearly in the EOF analyses cited above. The reasons for this apparent frequency dependence in the structure of the patterns are not well understood.

4. Coupled Variations in the Tropical Atlantic and Indian Ocean Sectors

The standard deviation of SST in the tropical Atlantic and Indian Oceans is only about half as large as over the equatorial Pacific [*Hsiung and Newell*, 1983; *Bottomley et al.*, 1990], and the ratio is even smaller if only the spatially coherent portion of the variability, exclusive of the ENSO signal, is considered. Nevertheless, by the early 1980s it was already clear that coupled ocean-atmosphere variability over the tropical Atlantic sector was capable of impacting monsoon rainfall over the neighboring continents. In recognition of these promising results and in hopes that similar relationships might emerge in the Indian Ocean sector the TOGA program was defined as encompassing all three tropical oceans.

EOF analyses of SST anomalies in the tropical Atlantic by *Weare* [1977], *Hastenrath* [1978], *Lough* [1986], *Servain and Legler* [1986], and *Servain* [1991] revealed an array of spatially coherent patterns, including what appears to be an analogue of the ENSO variability in the Pacific. In contrast to the Pacific, where the ENSO variability dominates, off-equatorial SST anomalies in the tropical Atlantic are comparable in amplitude to those observed in the equatorial cold tongue. The off-equatorial anomalies have often been characterized in terms of a dipole mode, centered about the climatological mean ITCZ. *Houghton and Tourre* [1992] have argued that they are more appropriately viewed as spatially coherent, but linearly independent, modes of variability in the northern and southern tropics.

Hisard [1980], *Merle* [1980], and *Merle et al.* [1980] showed that SST and subsurface temperatures in the Atlantic cold tongue region in the Gulf of Guinea exhibit interannual variability analogous to the ENSO cycle in the eastern Pacific, and *Hisard* [1980] presented evidence that El Niño-like events are accompanied by anomalously heavy August rainfall along the Ivory Coast. As in the Pacific, the equatorial oceanic anomalies are preceded by a weakening of the easterlies in the western part of the basin [*Servain et al.*, 1982; *Carton and Huang*, 1994]. *Horel et al.* [1986] and *Philander* [1986] have suggested that in some cases the wind anomalies appear to be a remote response to strong swings of the ENSO cycle in the Pacific. On the other hand, coupled modeling results of *Zebiak* [1993] suggest that the equatorial SST and wind anomalies could arise from coupled ocean-atmosphere interactions analogous to but distinct from those in the ENSO cycle. Studies of *Aceituno* [1988], *Curtis and Hastenrath* [1995], and *Nobre and Shukla* [1996] suggest that the remote forcing from the Pacific may also be responsible for some of the off-equatorial SST anomalies in the tropical Atlantic.

The off-equatorial SST anomalies are strongly correlated with rainfall anomalies over northeast Brazil [*Hastenrath and Heller*, 1977; *Markham and McLain*, 1977; *Moura and Shukla*, 1981] indicative of shifts of the ITCZ in the western Atlantic from its seasonally varying climatological mean position [*Hastenrath and Lamb*, 1977a, b; *Hastenrath and Greischar*, 1993]. They are accompanied by spatially coherent cross-equatorial surface wind anomalies [*Nobre and Shukla*, 1996], reminiscent of those observed in association with the climatological mean annual march [*Mitchell and Wallace*, 1992]. Plate 10 shows the patterns of rainfall, SST, SLP, and surface wind anomalies observed in association with positive rainfall anomalies over northeast Brazil during the rainy season February-May, based on regression analysis, as described in the Plate 10 caption. Near the Brazil coast the axis of symmetry of the surface wind pattern and the nodes in the rainfall, SST, and SLP patterns coincide with the climatological mean ITCZ. The patterns are dynamically consistent and indicative of a southward displacement of the ITCZ during the seasons with above normal rainfall in northeast Brazil. The SST anomalies are substantially weaker than those observed in the equatorial Pacific in association with ENSO, but the pattern is nonetheless quite robust, and there is ample evidence based on atmospheric general circulation model simulations that it is capable of forcing the observed rainfall anomalies [*Moura and Shukla*, 1981; *Mechoso et al.*, 1990]. The corresponding pattern for tropospheric-layer-averaged temperature (not shown) is much weaker and less distinct than its ENSO counterpart in Plate 7.

Anomalies in monsoon rainfall in sub-saharan West Africa have also been linked to SST anomalies in the tropical Atlantic [*Lamb*, 1978; *Folland et al.*, 1986; *Lough*, 1986; *Palmer*, 1986; *Semazzi et al.*, 1988; *Parker et al.*, 1988; *Lamb and Peppler*, 1991; *Rowell et al.*, 1995]. Above normal rainfall in this region tends to be associated with negative SST anomalies in the Gulf of Guinea and positive SST anomalies in the western Atlantic poleward of 15°N. The observed correlations are not as strong as those involving northeast Brazil rainfall, and their statistical significance is compromised by the marked decrease in rainfall over this region from the 1950s to the 1980s [*Nicholson*, 1993; *Rowell et al.*, 1995], which reduces the effective number of degrees of freedom inherent in the sub-saharan rainfall time series relative to the northeast Brazil series in Plate 10. Nevertheless, the statistical relationships appear to be physically plausible and analogous to those for northeast Brazil rainfall anomalies, and they have been replicated in atmospheric general circulation model (GCM) simulations with an early version of the United Kingdom Meteorological Office climate model [*Rowell et al.*, 1995].

The leading mode of SST variability in the tropical Indian Ocean is spatially amorphous and of the same polarity throughout the domain [*Weare*, 1979; *Navato et al.*, 1981]. Hence it is largely a reflection of variations in spatial mean temperature, whose variability is highly correlated with ENSO indices [*Bottomley et al.*, 1990; *Yulaeva and Wallace*, 1994]. The fact that fluctuations in Indian Ocean SST are lagged by about a season, relative to ENSO indices, suggests that they

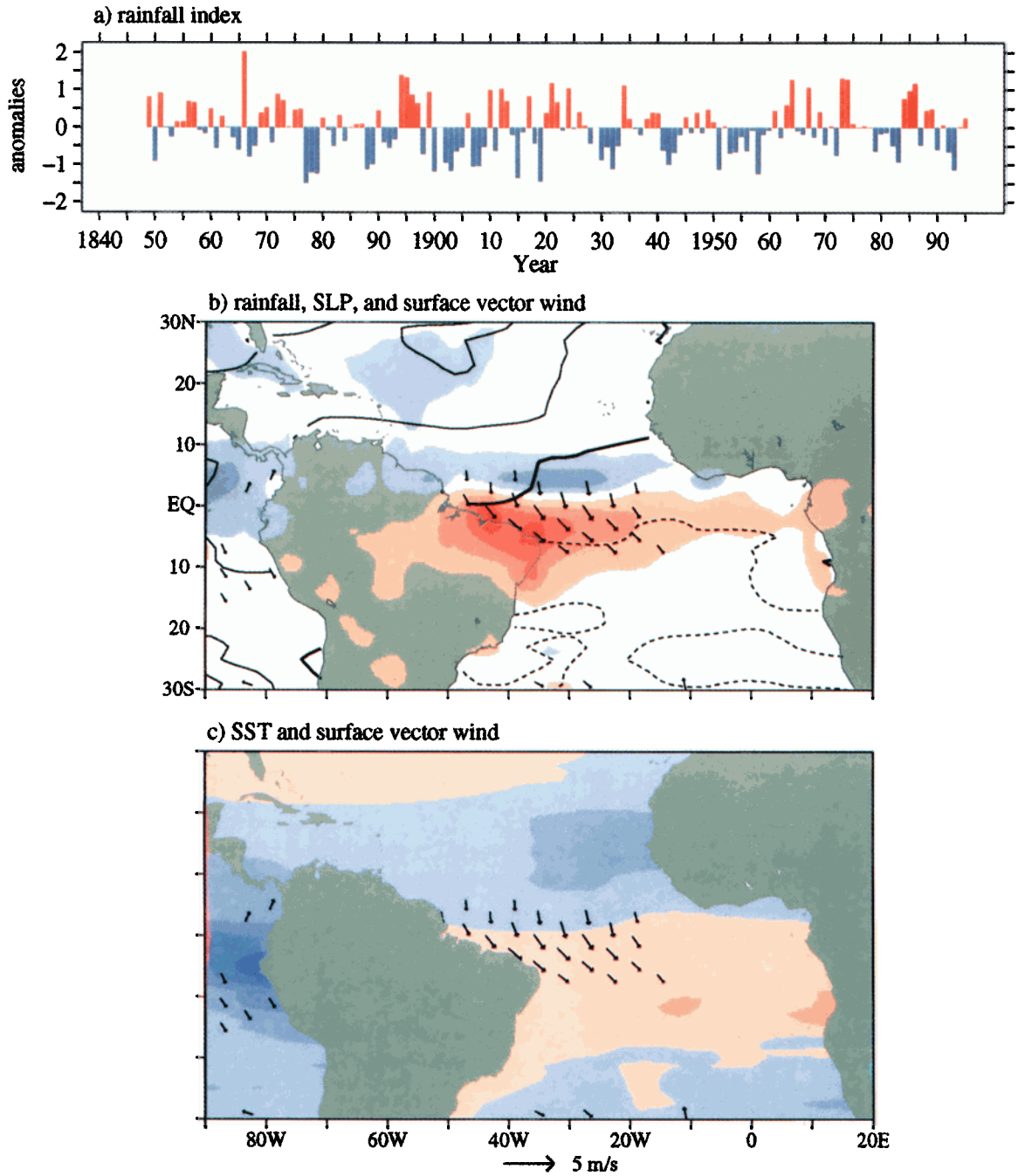

Plate 10. February through May northeast Brazil rainfall anomaly index for 1849–1995 and simultaneous regressions of selected seasonal mean fields onto this index for 1985-1993. (Rainfall index taken as the standardized average of standardized Fortaleza (3.7°S, 38.5°W) (1849-1987) and Quixeramobim (5.3°S, 39.3°W) (1896-1987) rainfall anomalies. Values for 1988-1995 were obtained from *Xie and Arkin* [1996].) (a) Anomalies are shown with respect to the entire period of record. (b) COADS SLP (contours) and COADS surface vector wind are superimposed upon rainfall (shading). (c) COADS surface vector wind is superimposed upon COADS SST. Shading and contouring conventions are as in Plate 7. Fortaleza and Quixeramobim rainfall time series were obtained from the World Monthly Surface Station Climatology from NCAR; rainfall fields are from NOAA/NCEP [*Xie and Arkin,* 1996].

occur in response to the ENSO cycle. This interpretation is supported by recent atmospheric GCM experiments *by Lau and Nath* [1994, 1996]. Spatial mean SST over the tropical Indian Ocean is strongly coupled with the interdecadal variability discussed in section 3.2 [*Nitta and Yamada*, 1989; *Kawamura,* 1994].

Indian rainfall exhibits only a weak correlation with SST upstream over the Arabian Sea [*Shukla and Misra*, 1977; *Weare* 1979]. It is more strongly (positively) correlated with the SOI [*Walker*, 1924; *Pant and Parthasarathy*, 1981] and averages significantly below normal during monsoon seasons that fall within warm episodes of the ENSO cycle as defined by

equatorial Pacific SST [*Rasmusson and Carpenter*, 1983]. Hence, in contrast to other tropical oceans, where SST and rainfall anomalies tend to be strongly coupled in a regional context, year-to-year variations in SST and rainfall over the Indian sector both appear to be remote responses to ENSO-related variability in the Pacific.

5. Lessons Learned From TOGA

The enhanced observations during the TOGA decade provided a clearer definition of the spatial patterns associated with the ENSO cycle than had hitherto been possible. The observed variability displayed many of the characteristics noted in the studies reviewed in section 2. Basin-wide SST variations centered in the equatorial waveguide were tightly coupled to variations in zonal wind centered near the date line. Basin-wide warm episodes were accompanied by a weakening of the equatorial easterlies, by incursions of heavy rainfall into the equatorial dry zone, and by a local enhancement of the equatorially symmetric Hadley Circulation in the Pacific sector. South American coastal warmings occurred in association with the basin-wide warm episodes, and they coincided with the climatological mean warm season centered around February-April. In comparison to prior estimates based upon OLR, the new rainfall products developed during TOGA tend to place greater emphasis upon the ITCZ and the associated rainfall anomalies to the east of the date line (Plate A1 and Figure A1). Instead of merely indicating an eastward shift of the belt of heavy rainfall over the western Pacific "warm pool" during warm episodes of the ENSO cycle, the new rainfall estimates indicate a major contraction of the equatorial dry zone. The planetary-scale atmospheric response to the rainfall anomalies exhibited the distinctive equatorially symmetric dipole pattern in tropospheric layer mean temperature and 200-hPa stream function identified in previous studies.

There were aspects of the variability during the TOGA decade that did not conform to the canonical El Niño scenario. Like its predecessor in 1982–1983, the 1986–1988 basin-wide warm episode was not preceded by a coastal El Niño event. Yet, despite the differences in sequencing, the seasonality inherent in the RC composite prevailed. Coastal El Niño events continued to be observed during the warm season, and equatorial rainfall anomalies tended to be most pronounced in December through April, as documented in Plate 3 and, in more detail, in work by *Mitchell and Wallace* [1996]. A more fundamental departure from the RC scenario is the lack of coherence between the sequence of warm and cold episodes in different parts of the tropical Pacific. There were times during the early 1990s when it was difficult to define the status

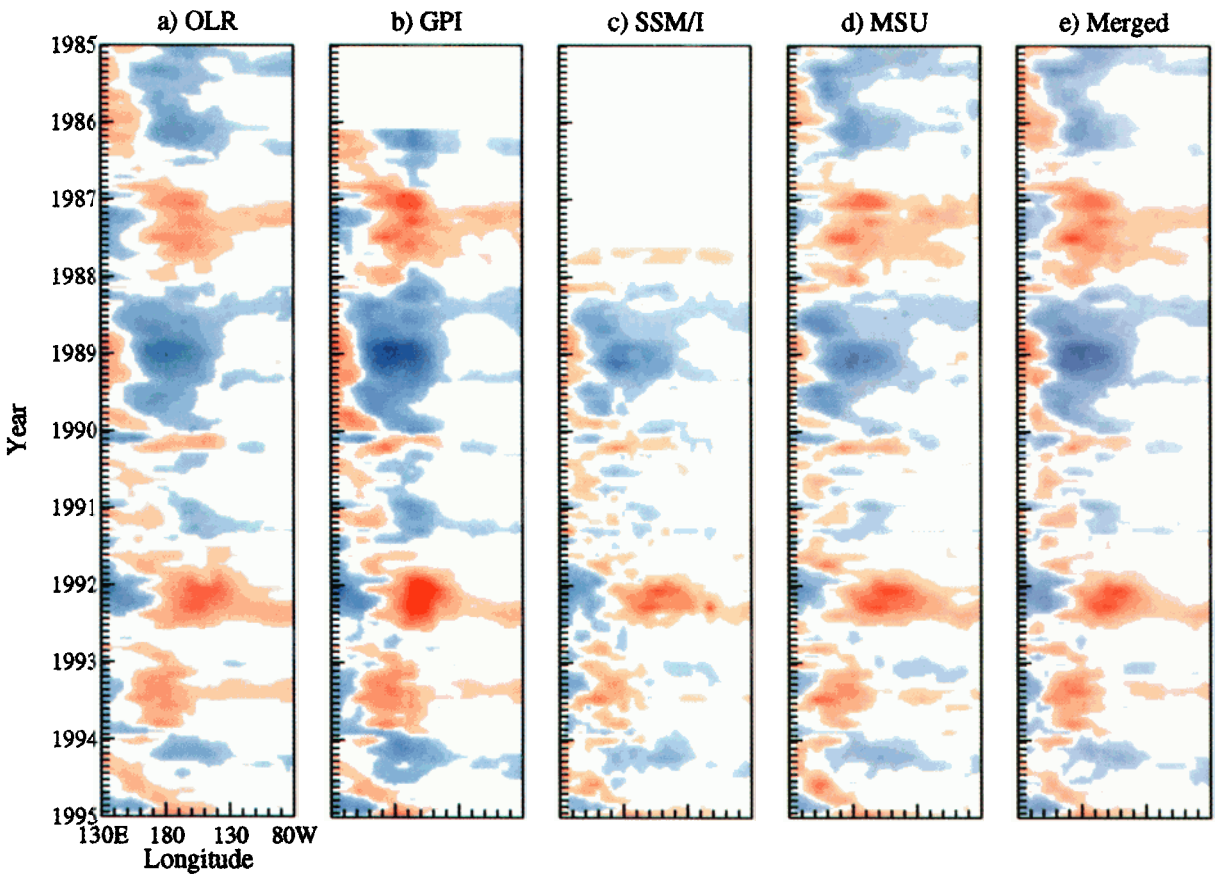

Plate A1. Time-longitude diagram of anomalies in OLR (8.75°N–11.25°S), GPI (7.5°N–10°S), SSM/I rainfall (10°N–10°S), MSU rainfall (7.5°N–10°S), and merged rainfall estimates (7.5°N–10°S). Red and blue shading are for positive and negative rainfall anomalies, respectively (negative and positive OLR anomalies, respectively). Light and saturated shading are for rainfall anomaly magnitudes > 2.5 and > 25.0 cm month^{-1}, respectively (OLR anomaly magnitudes > 5 and > 30 W m^{-2}, respectively). Data sources are OLR as in Plate 9, GPI and merged rainfall from NOAA/NCEP, SSM/I from NOAA/NESDIS, and MSU as in Plate 3.

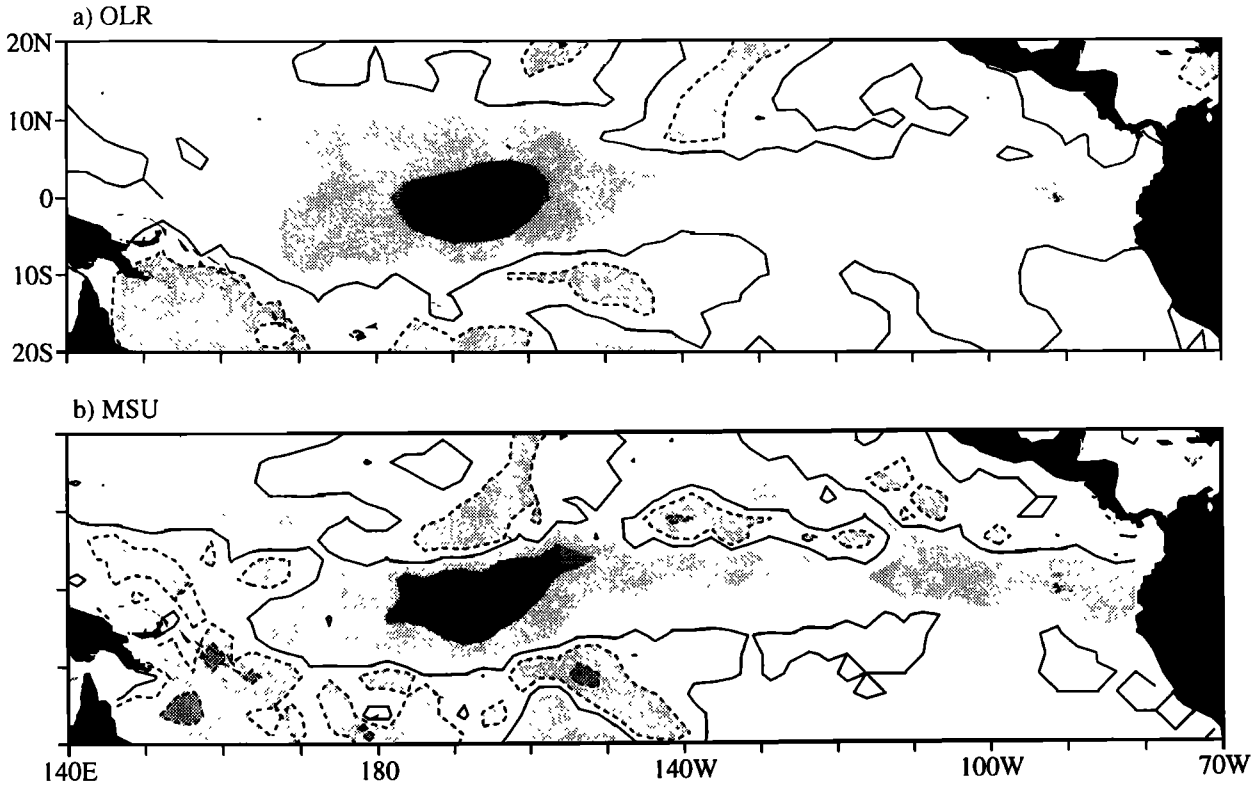

Figure A1. December-January-February averages for 1986–1987 minus 1988–1989 in (a) OLR and (b) MSU rainfall. Progressively darker shading for OLR anomalies > 10, 30, 50 W m^{-2} in magnitude and rainfall anomalies > 7.5, 22.5, 37.5 cm $month^{-1}$ in magnitude. Solid and dashed contours indicate no change and increases in OLR (decreases in MSU rainfall) from 1986–1987 to 1988–1989, respectively.

of the ENSO cycle; for example, some ENSO indices were indicative of the warm phase while others were indicative of the cold phase.

The ambiguity in the status of the ENSO cycle during the second half of the TOGA decade is related to the broadening of the frequency spectrum of ENSO-related variability. The unifying rhythm that permeated SST time series throughout the tropical Pacific during the much of the 1960s and 1970s was no longer in evidence. SST in the eastern equatorial Pacific exhibited high-frequency fluctuations with periods as short as a year while SST anomalies in the equatorial central Pacific and the off-equatorial eastern Pacific exhibited much greater year-to-year persistence. Aperiodic behavior is not unprecedented in the historical record: it was observed during the 1930s and 1940s [*Trenberth and Shea*, 1987]. Unfortunately, the ENSO variability during that period has received relatively little attention because of concerns about the reliability of SST observations prior to the 1950s. It has not been until quite recently that the scientific community has had the opportunity to diagnose well-documented ENSO-related variability in the absence of a dominant spatial pattern and rhythm.

Like the rhythms that characterize day-to-day weather fluctuations, the ENSO cycle fades in and out at irregular intervals. When it is strong, ENSO is likely to be more predictable [*Chen et al.*, 1995; *Davey et al.*, 1996; *Goddard and Graham*, 1997], and skillful forecasts are likely to be of more value, since it is the largest-amplitude ENSO-related climate anomalies that produce the most significant societal impacts.

TOGA did not reveal the existence of any previously undiscovered SST/rainfall connections over the other tropical oceans. The most robust of these linkages still appears to be the one between February-May rainfall over northeast Brazil and off-equatorial SST anomalies in the tropical Atlantic.

Appendix: Satellite Rainfall Estimates

Plate A1 presents time-longitude sections of Pacific rainfall estimates from OLR [*Chelliah and Arkin*, 1992], GPI [*Joyce and Arkin*, 1997], SSM/I [Ferraro et al., 1996], MSU [*Spencer*, 1993], and a blend of rain gauge, GPI, two SSM/I products, and prediction model output [*Xie and Arkin*, 1996] for the period 1985–1994. The meridional averages are taken for a band of latitudes centered slightly south of the equator to capture the largest ENSO-related east-west rainfall contrasts. The shading of OLR anomalies is chosen to be consistent with negative anomalies indicating greater than average rainfall. *Joyce and Arkin* [1997] present a similar comparison of GPI, MSU, and SSM/I rainfall. Figure A1 documents the difference in OLR and MSU rainfall for December-January-February averages for 1986–1987 minus 1988–1989, seasons which are representative of the large swings in rainfall amounts between ENSO warm and cold episodes.

Acknowledgments. This work was supported by the NOAA Climate and Global Change Program through a grant to the Hayes Center. The authors wish to thank Ants Leetmaa, Michael McPhaden, Sharon Nicholson, Sumant Nigam, Jagadish Shukla, and the reviewers for their contributions to this work. This is JISAO contribution 376.

References

Aceituno, P., On the functioning of the Southern Oscillation in the South American sector, I, Surface climate, *Mon. Weather Rev., 116*, 505-524, 1988.

Barber, R. T., and F. P. Chavez, Biological consequences of El Niño, *Science, 222*, 1203–1210, 1983.

Barnett, T. P., Interaction of the monsoon and Pacific trade wind system at interannual time scales, I, The equatorial zone, *Mon. Weather Rev., 111*, 756–773, 1983.

Bengtsson, L., and J. Shukla, Integration of space and in situ observations to study global climate change, *Bull. Am. Meteorol. Soc., 69*, 1130-1143, 1988.

Berlage, H. P., Fluctuations in the general atmospheric circulation of more than one year, their nature and prognostic value, *Meded. Verh.*, K. Ned. Meteorol. Inst., *88*, 152 pp., 1966.

Bjerknes, J., Atmospheric teleconnections from the equatorial Pacific, *Mon. Weather Rev., 18*, 820–829, 1969.

Bottomley, M., C. K. Folland, J. Hsiung, R. E. Newell, and D. E. Parker, Global Ocean Surface Temperature Atlas (GOSTA), 333 pp., Her Majesty's Stn. Off., Norwich, England, 1990.

Brooks, C. E. P., and H. W. Braby, The clash of the trades in the Pacific, *Q. J. R. Meteorol. Soc., 47*, 1–13, 1921.

Busalacchi, A., and J. J. O'Brien, Interannual variability of the equatorial Pacific in the 1960s, *J. Geophys. Res., 86*, 10,901–10,907, 1981.

Cane, M. A., Oceanographic events during El Niño, *Science, 222*, 1189–1195, 1983.

Cane, M. A., A. C. Clement, A. Kaplan, Y. Kushnir, D. Pozdnyakov, R. Seager, S. E. Zebiak, and R. Murtugudde, Twentieth century sea surface temperature trends, *Science, 275*, 957-960, 1997.

Carton, J. A., and B. Huang, Warm events in the tropical Atlantic, *J. Phys. Oceanogr., 24*, 888-903, 1994.

Chelliah, M., and P. A. Arkin, Large-scale interannual variability of outgoing longwave radiation anomalies over the global tropics, *J. Clim., 5*, 371–389, 1992.

Chen, D., S. E. Zebiak, A. J. Busalacchi, and M. A. Cane, An improved procedure for El Niño forecasting, *Science, 269*, 1699–1702, 1995.

Curtis, S., and S. Hastenrath, Forcing of anomalous sea surface temperature evolution in the tropical Atlantic during Pacific warm events, *J. Geophys. Res., 100*, 15,835-15,847, 1995.

Davey, M. K., D. L. T. Anderson, and S. Lawrence, A simulation of variability in ENSO forecast skill, *J. Clim., 9*, 240–246, 1996.

Deser, C., and J. M. Wallace, El Niño events and their relation to the Southern Oscillation: 1925–1986, *J. Geophys. Res., 92*, 14,189–14,196, 1987.

Doberitz, R., Cross-spectrum analysis of rainfall and sea temperature of the equatorial Pacific Ocean, *Bonner Meteorol. Abh., 8*, 61 pp., Bonn, 1968.

Eguiguren, D. V., Las nuivas de Piura, *Biol. Soc. Geogr. Lima, 4*, 241–258, 1894.

Ferraro, R. R., F. Weng, N. C. Grody, and A. Basist, An eight-year (1987-1994) time series of rainfall, clouds, water vapor, snow cover, and sea ice derived from SSM/I measurements, *Bull. Am. Meteorol. Soc., 77*, 891-905, 1996.

Folland, C. K., T. N. Palmer, and D. E. Parker, Sahel rainfall and worldwide sea temperatures, 1901-85, *Nature, 320*, 602-607, 1986.

Gadgil, S., P. V. Joseph, and N. V. Noshi, Ocean-atmosphere coupling over the monsoon regions, *Nature, 312*, 141-143, 1984.

Gibson, J. K., P. Kållberg, S. Uppala, A. Hernandez, A. Nomura, and E. Serrano, ECMWF re-analysis description, *ECMWF Re-Anal. Proj. Rep. Ser. 1*, 1-71, European Centre for Medium-Range Weather Forecasts, Reading, England, 1997.

Gill, A.E., Some simple solutions for heat-induced tropical circulation, *Q. J. R. Meteorol. Soc., 106*, 447-462, 1980.

Goddard, L., and N. E. Graham, El Niño in the 1990s, *J. Geophys. Res., 102*, 10,423-10,436, 1997.

Graham, N. E., Decadal-scale climate variability in the 1970s and 1980s: Observations and model results, *Clim. Dyn., 10*, 135–162, 1994.

Graham, N. E., and T. P. Barnett, Sea surface temperatures, surface wind divergence, and convection over the tropical oceans, *Science, 238*, 657-659, 1987.

Hastenrath, S., On modes of tropical circulation and climate anomalies, *J. Atmos. Sci., 35*, 2222-2231, 1978.

Hastenrath, S., and A. Greischar, Circulation mechanisms related to northeast Brazil rainfall anomalies, *J. Geophys. Res., 98*, 5093-5102, 1993.

Hastenrath, S., and L. Heller, On the modes of tropical circulation and climate anomalies, *Q. J. R. Meteorol. Soc., 103*, 77-92, 1977.

Hastenrath, S., and P. Lamb, *Climatic atlas of the tropical Atlantic and eastern Pacific Ocean*, 112 pp., Univ. of Wis. Press, Madison, 1977a.

Hastenrath, S., and P. Lamb, Some aspects of circulation and climate over the eastern equatorial Atlantic, *Mon. Weather Rev., 105*, 1019-1023, 1977b.

Hisard, P., Observation de réponses de type << El Niño>> dans l'Atlantique tropical oriental Golfe de Guineé, *Oceanol. Acta, 3*, 69-78, 1980.

Hoerling, M. P., A. Kumar, and M. Zhong, El Niño, La Niña, and the nonlinearity of their teleconnections, *J. Clim., 10*, 1769-1786, 1997.

Horel, J. D., On the annual cycle of the tropical Pacific atmosphere and ocean, *Mon. Weather Rev., 110*, 1863–1878, 1982.

Horel, J. D., V. E. Kousky, and M. T. Kagano, Atmospheric conditions in the Atlantic sector during 1983 and 1984, *Nature, 322*, 248-251, 1986.

Houghton, R. W., and Y. Tourre, Characteristics of low frequency SST fluctuations in the tropical Atlantic, *J. Clim., 5*, 765-771, 1992.

Hsiung, J., and R. E. Newell, The principal non-seasonal modes of global sea surface temperature, *J. Phys. Oceanogr., 13*, 1957-1967, 1983.

Hurlburt, H. E., J. C. Kindle, and J. J. O'Brien, A numerical simulation of the onset of El Niño, *J. Phys. Oceanogr., 6*, 621–631, 1976.

Ichiye, T., and J. Peterson, The anomalous rainfall of the 1957–58 winter in the equatorial central Pacific arid area, *J. Meteorol. Soc. Jpn., 41*, 172–182, 1963.

Joyce, R., and P. A. Arkin, Improved estimates of tropical and subtropical precipitation using the GOES precipitation index, *J. Atmos. Oceanic Technol., 14*, 997-1011, 1997.

Julian, P. R., and R. M. Chervin, A study of the Southern Oscillation and the Walker Circulation phenomenon, *Mon. Weather Rev., 106*, 1433–1451, 1978.

Kalnay, E., et al., The NCEP/NCAR 40-year reanalysis project, *Bull. Am. Meteorol. Soc., 77*, 437–471, 1996.

Kawamura, R., A rotated EOF analysis of global sea surface temperature variability with interannual and interdecadal scale, *J. Phys. Oceanogr., 24*, 707-715, 1994.

Lamb, P. J., Large-scale tropical Atlantic surface circulation patterns associated with Subsaharan weather anomalies, *Tellus, 30*, 241-251, 1978.

Lamb, P. J., and R. A. Peppler, West Africa, in *Teleconnections Linking Worldwide Climate Anomalies*, edited by M. H. Glantz, R. W. Katz, and N. Nicholls, pp. 121-189, Cambridge Univ. Press, 1991.

Lau, N.-C., and M. J. Nath, A modeling study of the relative roles of tropical and extratropical SST anomalies in the variability of the global atmosphere-ocean system, *J. Clim., 7*, 1184-1207, 1994.

Lau, N.-C., and M. J. Nath, The role of the "Atmospheric Bridge" in linking tropical Pacific ENSO events to extratropical SST anomalies, *J. Clim., 9*, 2036-2057, 1996.

Leighly, J. B., Marquesan meteorology, *Univ. Calif. Publ. Geogr., 6(4)*, 147–172, 1933.

Lobell, M. J., Some observations on the Peruvian coastal current, *EOS Trans. AGU, 23*, 332–336, 1942.

Lough, J. M., Tropical Atlantic sea surface temperatures and rainfall variations in Subsaharan Africa, *Mon. Weather Rev., 114*, 561-570, 1986.

Markham, C. G., and D. R. McLain, Sea surface temperature related to rain in Ceará, northeast Brazil, *Nature, 265*, 320-323, 1977.

Matsuno, T., Quasi-geostrophic motions in the equatorial area, *J. Meteorol. Soc. Jpn., 44*, 25-43, 1966.

McCreary, J. P., Eastern tropical ocean response to changing wind systems with application to El Niño, *J. Phys. Oceanogr., 6*, 632-645, 1976.

McPhaden, M. J., and J. Picaut, El Niño-Southern Oscillation displacements of the western equatorial Pacific warm pool, *Science, 250*, 1385-1388, 1990.

McPhaden, M. J., et al., Tropical Ocean–Global Atmosphere observing system: A decade of progress, *J. Geophys. Res.*, this issue.

McWilliams, J. C., and P. R. Gent, A coupled air-sea model for the tropical Pacific, *J. Atmos. Sci., 35*, 962–989, 1978.

Mechoso, C. R., S. W. Lyons, and J. A. Spahr, The impact of sea surface temperature anomalies on the rainfall over northeast Brazil, *J. Clim., 3*, 812-826, 1990.

Merle, J., Variabilité thermique annuelle et interannuelle de l'ocean Atlantique équatorial Est. L'hypothé se d'un <<El Niño>> Atlantique, *Oceanol. Acta, 3*, 209-220, 1980.

Merle, J., M. Fieux, and P. Hisard, Annual cycle and interannual anomalies of sea surface temperature in the eastern equatorial Atlantic Ocean, *Deep Sea Res., Part A, 26*, 77-101, 1980.

Mitchell, T. P., and J. M. Wallace, The annual cycle in equatorial convection and sea surface temperature, *J. Clim., 5*, 1140-1156, 1992.

Mitchell, T. P., and J. M. Wallace, An observational study of ENSO variability in 1950–78 and 1979–92, *J. Clim., 9*, 3149-3161, 1996.

Moura, A. D., and J. Shukla, On the dynamics of droughts in northeast Brazil: Observations, theory and numerical experiments with a general circulation model, *J. Atmos. Sci., 38*, 2653-2675, 1981.

Murphy, R. C., Oceanic and climatic phenomena along the west coast of South America during 1925, *Geogr. Rev., 16*, 25–54, 1926.

Navato, A. R., R. E. Newell, J. C. Hsiung, C. B. Billing, and B. Weare, Tropospheric mean temperature and its relationship to the oceans and atmospheric aerosols, *Mon. Weather Rev., 109*, 244-254, 1981.

Nicholson, S. E., An overview of African rainfall fluctuations of the last decade, *J. Clim., 6*, 1463-1466, 1993.

Nitta, T., and S. Yamada, Recent warming of tropical sea surface temperature and its relationship to the northern hemisphere circulation, *J. Meteorol. Soc. Jpn., 67*, 375–383, 1989.

Nobre, P., and J. Shukla, Variations of sea surface temperature, wind stress, and rainfall over the tropical Atlantic and South America, *J. Clim., 9*, 2464-2479, 1996.

Palmer, T. N., Influence of the Atlantic, Pacific and Indian Oceans on Sahel rainfall, *Nature, 322*, 251-253, 1986.

Pant, G. B., and B. Parthasarathy, Some aspects of an association between the Southern Oscillation and Indian summer monsoon, *Arch. Meteorol. Geophys. Bioklimatol., Ser. B, 29*, 245-252, 1981.

Parker, D. E., C. K. Folland, and M. N. Ward, Sea surface temperature anomaly patterns and prediction of seasonal rainfall in the Sahel region of Africa, in *Recent Climate Change: A Regional Approach*, edited by S. Gregory, pp. 166-178, Belhaven, London, 1988.

Pazan, S., and G. Meyers, Interannual fluctuations in the tropical Pacific wind field and the Southern Oscillation, *Mon. Weather Rev., 110*, 587–600, 1982.

Philander, S. G. H., Unusual conditions in the tropical Atlantic in 1984, *Nature, 322*, 236-238, 1986.

Picaut, J., M. Ioualelen, C. Menkes, T. Delcroix, and M. J. McPhaden, Mechanism of the zonal displacements of the Pacific warm pool: Implications for ENSO, *Science, 274*, 1486-1489, 1996.

Poulain, P. -M., Estimates of horizontal divergence and vertical velocity in the equatorial Pacific, *J. Phys. Oceanogr., 23*, 601–607, 1993.

Quinn, W. H., D. O. Zopf, K. S. Short, and R. W. T. Kuo Yang, Historical trends and statistics of the Southern Oscillation, El Niño, and Indonesian droughts, *Fish. Bull., 76*, 663–678, 1978.

Ramage, C. S., and A. M. Hori, Meteorological aspects of El Niño, *Mon. Weather Rev., 109*, 1827–1835, 1981.

Rasmusson, E. M., and T. H. Carpenter, Variations in the tropical sea surface temperature and surface wind fields associated with the Southern Oscillation/El Niño, *Mon. Weather Rev., 110*, 354–384, 1982.

Rasmusson, E. M., and T. H. Carpenter, The relationship between eastern equatorial Pacific sea surface temperatures and rainfall over India and Sri Lanka, *Mon. Weather Rev., 111*, 517-528, 1983.

Rasmusson, E. M., and J. M. Wallace, Meteorological aspects of the El Niño/Southern Oscillation, *Science, 222*, 1195–1202, 1983.

Rasmusson, E. M., X. Wang, and C. F. Ropelewski, The biennial component of ENSO variability, *J. Mar. Syst., 1*, 71–96, 1990.

Reynolds, R. J., and T. M. Smith, Improved global sea surface temperature analyses using optimal interpolation, *J. Clim., 7*, 929–948, 1994.

Rowell, D. P., C. K. Folland, K. Maskell, and M. N. Ward, Variability of summer rainfall over tropical north Africa (1906-92): Observations and modelling, *Q. J. R. Meteorol. Soc., 121*, 669-704, 1995.

Schubert, S. D., R. B. Rood, and J. Pfaendtner, An assimilated dataset for earth science applications, *Bull. Am. Meteorol. Soc., 74*, 2331-2342, 1993.

Semazzi, F. H. M., V. Mehta, and Y. C. Sud, An investigation of the relationship between Sub-Saharan rainfall and global sea surface temperatures, *Atmos.Ocean, 26*, 118-138, 1988.

Servain, J., Simple climatic indices for the tropical Atlantic Ocean and some applications, *J. Geophys. Res., 96*, 15,137-15,146, 1991.

Servain, J., and D. M. Legler, Empirical orthogonal function analysis of tropical Atlantic sea surface temperature and wind stress: 1964-1979, *J. Geophys. Res., 91*, 14,181-14,191, 1986.

Servain, J., J. Picaut, and J. Merle, Evidence of remote forcing in the equatorial Atlantic, *J. Phys. Oceanogr., 12*, 457-463, 1982.

Shukla, J., and B. M. Misra, Relationships between sea-surface temperature and wind speed over the Arabian Sea and monsoon rainfall over India, *Mon. Weather Rev., 105*, 998-1002, 1977.

Smith, T. M., R. W. Reynolds, R. E. Livezey, and D. C. Stokes, Reconstruction of historical sea surface temperatures using empirical orthogonal functions, *J. Clim., 9*, 1403-1420, 1996.

Spencer, R. W., Global oceanic precipitation from the MSU during 1979–91 and comparisons to other climatologies, *J. Clim., 6*, 1301–1326, 1993.

Spencer, R. W., and J. Christy, Precise monitoring of global temperature trends from satellites, *Science, 247*, 1558–1562, 1990.

Spencer, R. W., and J. Christy, Precision and radiosonde validation of satellite gridpoint temperature anomalies, I, MSU channel 2, *J. Clim., 5*, 847–857, 1992.

Spencer, R. W., and J. Christy, Precision lower stratospheric monitoring with the MSU: Technique, validation, and results, 1979–91, *J. Clim., 6*, 1194–1204, 1993.

Stricherz, J., J. J. O'Brien, and D. M. Legler, *Atlas of Florida State University Tropical Pacific Winds for TOGA 1966–1985*, 250 pp., Fla. State Univ., Tallahassee, 1992.

Trenberth, K. E., Spatial and temporal variations in the Southern Oscillation, *Q. J. R. Meteorol. Soc., 102*, 639–653, 1976.

Trenberth, K. E., and T. J. Hoar, The 1990–1995 El Niño Southern Oscillation event: Longest on record, *Geophys. Res. Lett., 23*, 57–60, 1996.

Trenberth, K. E., and D. J. Shea, On the evolution of the Southern Oscillation, *Mon. Weather Rev., 115*, 3078-3096, 1987.

van Loon, H., and R. A. Madden, The Southern Oscillation, I, Global associations with pressure and temperature in northern winter, *Mon. Weather Rev., 109*, 1150–1672, 1981.

Walker, G. T., Correlation of seasonal variations in weather IX: A further study of world weather, *Mem. Indian Meteorol. Dep., 24*, 275–332, 1924.

Wallace, J. M., T. P. Mitchell, and C. Deser, The influence of sea surface temperature on surface wind in the eastern equatorial Pacific: Seasonal and interannual variability, *J. Clim., 2*, 1492-1499, 1989.

Wang, B., Interdecadal changes in El Niño onset in the last four decades, *J. Clim., 8*, 267–285, 1995.

Weare, B. C., Empirical orthogonal function analysis of Atlantic surface temperatures, *Q. J. R. Meteorol. Soc., 193*, 467-478, 1977.

Weare, B. C., A statistical study of the relationship between ocean temperature and the Indian monsoon., *J. Atmos. Sci., 36*, 2279-2291, 1979.

Weare, B. C., El Niño and tropical Pacific Ocean temperature, *J. Phys. Oceanogr., 12*, 17–27, 1982.

Weare, B. C., A. R. Navato, and R. E. Newell, Empirical orthogonal function analysis of Pacific sea surface temperatures, *J. Phys. Oceanogr., 6*, 671-678, 1976.

Webster, P. J., Response of the tropical atmosphere to local, steady forcing, *Mon. Weather Rev., 100*, 518-541, 1972.

Woodruff, S. D., R. J. Slutz, R. L. Jenne, and P. M. Steurer, A comprehensive ocean-atmosphere data set, *Bull. Am. Meteorol. Soc., 68*, 1239–1250, 1987.

Woodruff, S. D., S. J. Lubker, K. Wolter, S. J. Worley, and J. D. Elms, Comprehensive Ocean-Atmosphere Data Set (COADS) release 1a: 1980–92, *Earth Syst. Monit., 4*, 1-8, 1993.

Wooster, W. W., and O. Guillen, Characteristics of El Niño in 1972, *J. Mar. Res., 32*, 378–404, 1974.

Wright, P. B., The Southern Oscillation - Patterns and mechanisms of the teleconnections and the persistence, *Rep. HIG-77-13*, 107 pp., Hawaii Inst. Geophys., Univ.of Hawaii, Honolulu, 1977.

Wright, P. B., J. M. Wallace, T. P. Mitchell, and C. Deser, Correlation structure of the El Niño/Southern Oscillation phenomenon, *J. Clim., 1*, 609–625, 1988.

Wyrtki, K., The annual and semiannual variation of SST in the North Pacific Ocean, *Limnol. Oceanogr., 10*, 307–313, 1965.

Wyrtki, K., El Niño – The dynamic response of the equatorial Pacific Ocean to atmospheric forcing, *J. Phys. Oceanogr., 5*, 572–584, 1975.

Wyrtki, K., The response of sea level topography to the 1976 El Niño, *J. Phys. Oceanogr., 9*, 1223–1231, 1979.

Xie, P., and P. A. Arkin, Analyses of global monthly precipitation using gauge observations, satellite estimates, and numerical model predictions, *J. Clim., 9*, 840–858, 1996.

Yukimoto, S., M. Endoh, Y. Kitamura, A. Kitoh, T. Motoi, A. Noda, and T. Tokioka, Interannual and interdecadal variabilities in the Pacific in an MRI coupled GCM, *Clim. Dyn., 12*, 667-683, 1996.

Yulaeva, E., and J. M. Wallace, The signature of ENSO in global temperature and precipitation fields derived from the microwave sounding unit, *J. Clim., 7*, 1719–1736, 1994.

Zebiak, S. E., Air-sea interaction in the equatorial Atlantic region, *J. Clim., 6*, 1567-1586, 1993.

Zhang, Y., J. M. Wallace, and D. S. Battisti, ENSO-like interdecadal variability: 1900–93, *J. Clim., 10*, 1003-1020, 1997.

V. E. Kousky, NOAA/NCEP Climate Prediction Center, Washington, D. C. 20233.

T. P. Mitchell, E. S. Sarachik, and J. M. Wallace, Joint Institute for the Study of the Atmosphere and Ocean, Box 354235, University of Washington, Seattle, WA 98195-4235.

E. M. Rasmusson, Department of Meteorology, University of Maryland, College Park, MD 20742.

H. von Storch, Institute of Hydrophysics, GKSS, Max-Planck-Strasse 1, 21502 Geesthacht, Germany.

(Received June 21, 1996; revised October 8, 1997;
accepted October 10, 1997.)